BOREAS An international journal of Quaternary research

The Langeland Fault System unravelled: Quaternary fault reactivation along an elevated basement block between the North German and Norwegian–Danish basins

NIKLAS AHLRICHS, CHRISTIAN HÜBSCHER, THEIS RAASCHOU ANDERSEN, JONAS PREINE, LAURA BOGNER AND WIEBKE SCHÄFER

BOREAS

Ahlrichs, N., Hübscher, C., Andersen, T. R., Preine, J., Bogner, L. & Schäfer, W. 2023 (July): The Langeland Fault System unravelled: Quaternary fault reactivation along an elevated basement block between the North German and Norwegian–Danish basins. *Boreas*, Vol. 52, pp. 381–401. https://doi.org/10.1111/bor.12614. ISSN 0300-9483.

The reactivation of faults and possible impact on barrier integrity marks a critical aspect for investigations on subsurface usage capabilities. Glacial isostatic adjustments, originating from repeated Quaternary glaciations of northern Europe, cause tectonic stresses on pre-existing fault systems and structural elements of the North German and Norwegian–Danish basins. Notably, our current understanding of the dynamics and scales of glacially induced fault reactivation is rather limited. A high-resolution 2D seismic data set recently acquired offshore northeastern Langeland Island allows the investigation of a fault and graben system termed the Langeland Fault System. Seismo-stratigraphic interpretation of reflection seismic data in combination with diffraction imaging unravels the spatial character of the Langeland Fault System along an elevated basement block of the Ringkøbing–Fyn High. In combination with sediment echosounder data, the data set helps to visualize the continuation of deep-rooted faults up to the sea floor. Initial Mesozoic faulting occurred during the Triassic. Late Cretaceous inversion reactivated a basement fault flanking the southern border of the elevated basement block of the Ringkøbing–Fyn High while inversion is absent in the Langeland Fault System. Here, normal faulting occurred in the Maastrichtian–Danian. We show that a glacial or postglacial fault reactivation occurred within the Langeland Fault System, as evident by the propagation of the faults from the deeper subsurface up to the sea floor, dissecting glacial and postglacial successions. Our findings suggest that the Langeland Fault System was reactivated over a length scale of a minimum of 8.5 km. We discuss the causes for this Quaternary fault reactivations in the context of glacially induced faulting and the present-day stress field. The combination of imaging techniques with different penetration depths and vertical resolution used in this study is rarely realized in the hinterland. It can therefore be speculated that many more inherited, deep-rooted faults were reactivated in Pleistocene glaciated regions.

Niklas Ahlrichs (niklas.ahlrichs@uni-hamburg.de), Christian Hübscher, Jonas Preine, Laura Bogner and Wiebke Schäfer, Institute of Geophysics, Center for Earth System Research and Sustainability, Universität Hamburg, Hamburg 20146, Germany; Theis Raaschou Andersen, Research Center for Built Environment, Energy, Water and Climate, VIA University College, Horsens 8700, Denmark; *received 30th August 2022, accepted 19th January 2023.*

Good understanding of the subsurface and the tectonic developments shaping its present-day structural architecture is important for investigations concerning sustainable groundwater management or subsurface use capabilities (e.g. for Carbon Capture and Storage or as a repository of nuclear waste). Hence, the presence of faults plays an important role as the impact of tectonic stress is localized along weak zones, leading to the reactivation of preexisting faults rather than the development of new ones (White *et al*. 1986). The present knowledge about the possible impact of future tectonic activity would greatly benefit from an investigation of the neotectonic shallow fault reactivation and its connection with deep-rooted tectonic structures. The well-studied North German and Norwegian–Danish basins, where several studies reported recent fault movement induced by glacial isostatic adjustments, is a key area to gain insight into neotectonic processes and their relation to the deeper subsurface (see e.g. overviews of glacial induced faulting in Germany and Denmark by Müller *et al*. (2021) and Sandersen *et al*. (2021)). Over the past few decades, the Danish government has carried out a nationwide mapping campaign to identify groundwater protection sites (Thomsen *et al*. 2004). Within the scope of an airborne electromagnetic survey across Langeland Island, a shallow normal fault and graben system was detected in the northern part of the island (Fig. 1) (Andersen *et al*. 2016). Seismic data acquired offshore the northeastern coast of Langeland revealed a graben bound by conjugate faults, dissecting the Triassic to Quaternary successions reaching up to the sea floor (Al Hseinat & Hübscher 2017). Thereby, these authors interpreted the upward propagation of the faults across the Quaternary successions as an indication for recent fault reactivation related to the combined stress of glacial isostatic adjustments and the present-day stress field. However, given the lack of additional seismic data, which is crucial for understanding the dynamics and scale of glacially induced fault reactivations, it was not possible to further elaborate on the timing and context of the faulting within this study's structural framework.

The detected fault and graben system is in the northern part of Langeland Island, which is situated at the transition of the North German Basin in the south to the Norwegian–Danish Basin in the north (Fig. 1). These basins are part of the Central European Basin

DOI 10.1111/bor.12614

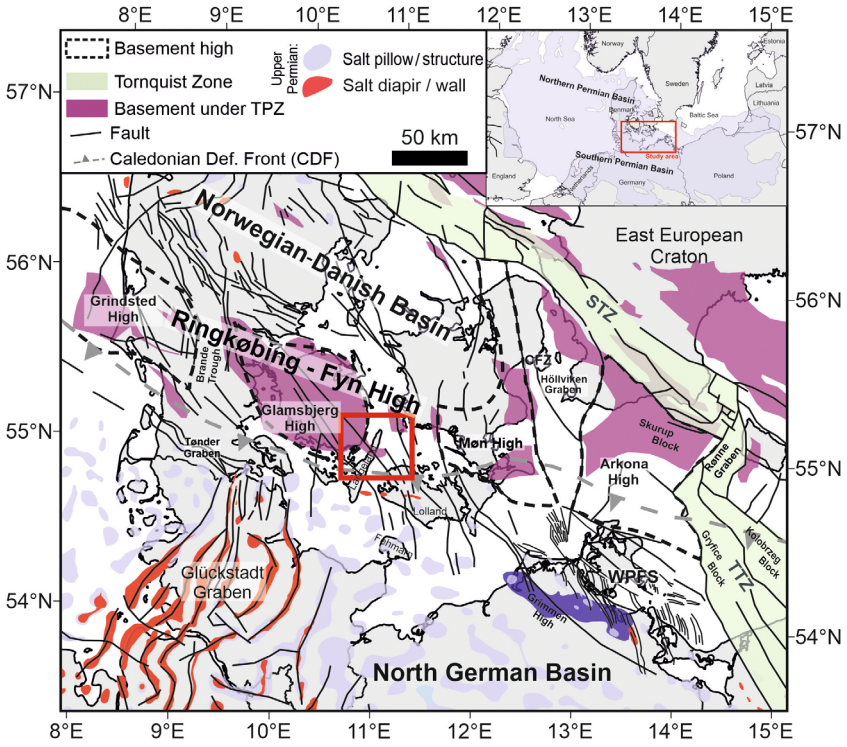

Fig. 1. Structural overview of Langeland Island within the tectonic framework of the North German and Norwegian–Danish basins (compiled after Vejbæk 1997; Ahlrichs *et al.* 2021, 2022 and references therein). Purple areas mark zones where the basement rests directly underneath the Top PreZechstein. Salt structures were compiled after Vejbæk (1997), Dadlez & Marek (1998), Reinhold *et al.* (2008), Warsitzka *et al.* (2019) and Ahlrichs *et al.* (2021). The inset shows the outline of the Central European Basin System. STZ = Sorgenfrei–Tornquist Zone; TTZ = Teisseyre–Tornquist Zone; WPFS = Western Pomeranian Fault System.

System, a series of intracontinental sedimentary basins with a long and complex history of basin evolution from Carboniferous to Quaternary (inset in Fig. 1, see e.g. overviews of Ziegler 1990; Maystrenko *et al.* 2008; Pharaoh *et al.* 2010). The sedimentary basins rest upon a complex crustal assemblage, the Palaeozoic Platform, which consists of Caledonian to Variscan consolidated crustal terranes and their transition to the Precambrian East European Craton (Fig. 1) (e.g. Guterch *et al.* 2010). This transition is termed the Trans-European Suture Zone and is spatially confined by the Caledonian Deformation Front in the north and the Elbe Line in the south (Berthelsen 1992; Guterch *et al.* 2010). The major structural elements in the context of this intracontinental sedimentary basin system are the Ringkøbing Fyn High (RFH), a series of basement highs between the North German and Norwegian–Danish basins, the Tornquist Zone, which is subdivided into the southern Teisseyre–Tornquist Zone and the northern Sorgenfrei–Tornquist Zone, and the Tornquist Fan, a northwestward widening zone of dominantly Palaeozoic faults south of the Tornquist Zone (Fig. 1) (EUGENO-S Working Group 1988; Berthelsen 1992; Thybo 1997; Vejbæk 1997).

The presence of a shallow fault and graben system for which a previous study suggested Quaternary fault reactivation (Al Hseinat & Hübscher 2017) and its location at the transition of the North German and Norwegian–Danish basins, makes the offshore area of Langeland Island an ideal study area to investigate neotectonics and fault reactivation by glacial isostatic adjustments (*sensu* Wu & Peltier 1982; Steffen *et al.* 2021a) in the context of the structural framework of a complex sedimentary basin system. Recently acquired marine seismic and sediment echosounder data offshore northeastern Langeland Island allow the identification and characterization of the offshore prolongation of the onshore Langeland detected fault and graben system. By a combination of these data sets with different target depths (sediment echosounder data – very shallow subsurface, a few metres; multichannel seismic data – depth of several kilometres), we strive for a comprehensive interpretation of Triassic to Quaternary subsurface evolution including recent fault reactivation within the structural framework of deep-rooted structures. Additionally, we use diffraction imaging to identify shallow faults and verify fault geometry observed from seismic reflection data. We aim to unravel fault reactivation of a deep-rooted fault system from Mesozoic to recent times involving Late Triassic extension, Late Cretaceous inversion and Quaternary fault reactivation. A major goal of this study is to contribute to a better understanding of neotectonics,

glacially induced faulting and the influence of precursor structures on fault reactivation, which is of great interest for investigations concerning barrier integrity in any subsurface usage projects.

Geological setting

The study area is located at the transition between the North German Basin in the south and Norwegian–Danish Basin in the north. The major structural element defining this marginal area between the basins is the RFH, an approximately WNW–ESE-striking set of basement highs (*sensu* Peacock & Banks 2020) consisting of the Grindsted High, Glamsbjerg High, Møn High and Arkona High (according to the nomenclature used by Vejbæk 1997; Fig. 1). Our study area is located between the Glamsbjerg and Møn highs, where a narrow branch of elevated basement that is connected to the Glamsbjerg High strikes east–west across Langeland Island (Fig. 1). The RFH was formed during the pre-Zechstein extension, driven by late Carboniferous–early Permian dextral strike-slip movements within the Trans-European Suture Zone, during which the RFH experienced less stretching than the adjacent subsiding North German and Norwegian–Danish basins (Thybo 1997, 2001; Vejbæk 1997; Clausen & Pedersen 1999). Accordingly, in most parts of the highs, the crystalline basement is relatively shallow and directly underlies the top pre-Zechstein horizon (Fig. 1) (Vejbæk 1997; Clausen & Pedersen 1999). During the late Permian, several marine transgressions at palaeogeographical low latitudes led to evaporation and the deposition of the Zechstein evaporites, which formed numerous salt structures within the North German and Norwegian–Danish basins during the Mesozoic–Cenozoic (e.g. Maystrenko *et al.* 2008; Fig. 1). Within the study area, only a thin Zechstein succession with carbonate-dominated marginal facies was deposited, and the lack of mobile halite hampered the development of salt structures (Stemmerik *et al.* 1987).

During the Triassic, the RFH continued to slowly subside, whereas the rapid subsidence of the North German and Norwegian–Danish basins amplified the differential subsidence leading to the thinning of the Triassic successions across the RFH (Buntsandstein, Muschelkalk and Keuper; see Fig. 2 for correlation with Danish lithostratigraphy) (Clausen & Pedersen 1999; Sachse & Littke 2016). From Middle to Late Jurassic times, the study area was affected by regional uplift related to thermal doming centred in the North Sea (Underhill 1998; Graversen 2006). Corresponding non-deposition and erosion caused the complete absence of Jurassic and partial removal of Triassic deposits (Fig. 2) (Michelsen 1978; Bertelsen 1980). Sedimentation resumed in the Albian followed by relatively quiet tectonic conditions characterized by the deposition of the Upper Cretaceous chalks (Fig. 2) (Cartwright 1990; Vejbæk *et al.* 2010). The onset of the Africa–Iberia–Europe convergence in the Late Cretaceous (Turonian/Coniacian until late Campanian) resulted in NW–SE to north–south directed shortening within the European foreland causing basin inversion, inversion of normal faults and reverse faulting within the North German and Norwegian–Danish basins (Vejbæk & Andersen 2002; Kockel 2003; Kley & Voigt 2008; Ahlrichs *et al.* 2021; Hansen *et al.* 2021). Further, shortening induced inversion of the normal faults within the Tornquist Fan and inversion, fault reactivation and uplift along the Sorgenfrei–Tornquist Zone, resulting in thinned or absent Upper Cretaceous chalk deposits (Erlström *et al.* 1997; Erlström & Sivhed 2001; Thybo 2001). During Maastrichtian times, the RFH remained a topographic high with deposition in shallow marine conditions (Thomsen 1974).

Large-scale domal uplift in the Paleocene removed Selandian sediments and partly Danian chalk in the Baltic sector of the North German Basin and its margin (Ahlrichs *et al.* 2021; von Eynatten *et al.* 2021). Hence, the present-day distribution boundary of Danian chalk is in the vicinity of our study area (Vinken & International Geological Correlation Programme 1988). Sediments deposited during the Eocene to Pliocene have mostly been eroded as a result of the Neogene uplift (Japsen *et al.* 2002, 2007; Rasmussen 2009).

During the Quaternary, the study area was covered by several ice sheets originating from the Scandinavian highlands throughout at least three major glaciations (e.g. Houmark-Nielsen 1987; Hughes *et al.* 2016). During the cyclical ice advance and retreat, the drainage of meltwater and glacial erosion removed the underlying pre-glacial Quaternary and Neogene sediments, incised Quaternary valleys into the pre-Quaternary subsurface, and deposited tills, sand and clay (e.g. Bennike *et al.* 2004; Ehlers *et al.* 2004; Eiriksson *et al.* 2006; Jørgensen & Sandersen 2006). Since the final decay of the Weichselian ice sheet, sedimentation is strongly controlled by eustatic sea-level changes and isostatic vertical motions (Björk 1995). During the postglacial Baltic Ice Lake, Yoldia Sea and early Ancylus Lake stages, our study area was located onshore, as it experienced isostatic uplift and the drainage of meltwater was situated within the Øresund area (Björk 1995). With the Ancylus Transgression, drainage along the Mecklenburg Bay and Fehmarn into the Storebælt began; this led to the development of the Dana River, eroding a prominent present-day submarine channel offshore eastern Langeland (Winn 1974; Björk 1995). Littorina and post-Littorina Sea sediments mark the major phase of postglacial sedimentation in the study area (Winn 1974). Present-day sedimentation is almost negligible (Winn 1974).

Database and methods

The data set used in this study consists of about 500 km of high-resolution, 2D reflection seismic data and equal profile lengths of parametric sediment echosounder

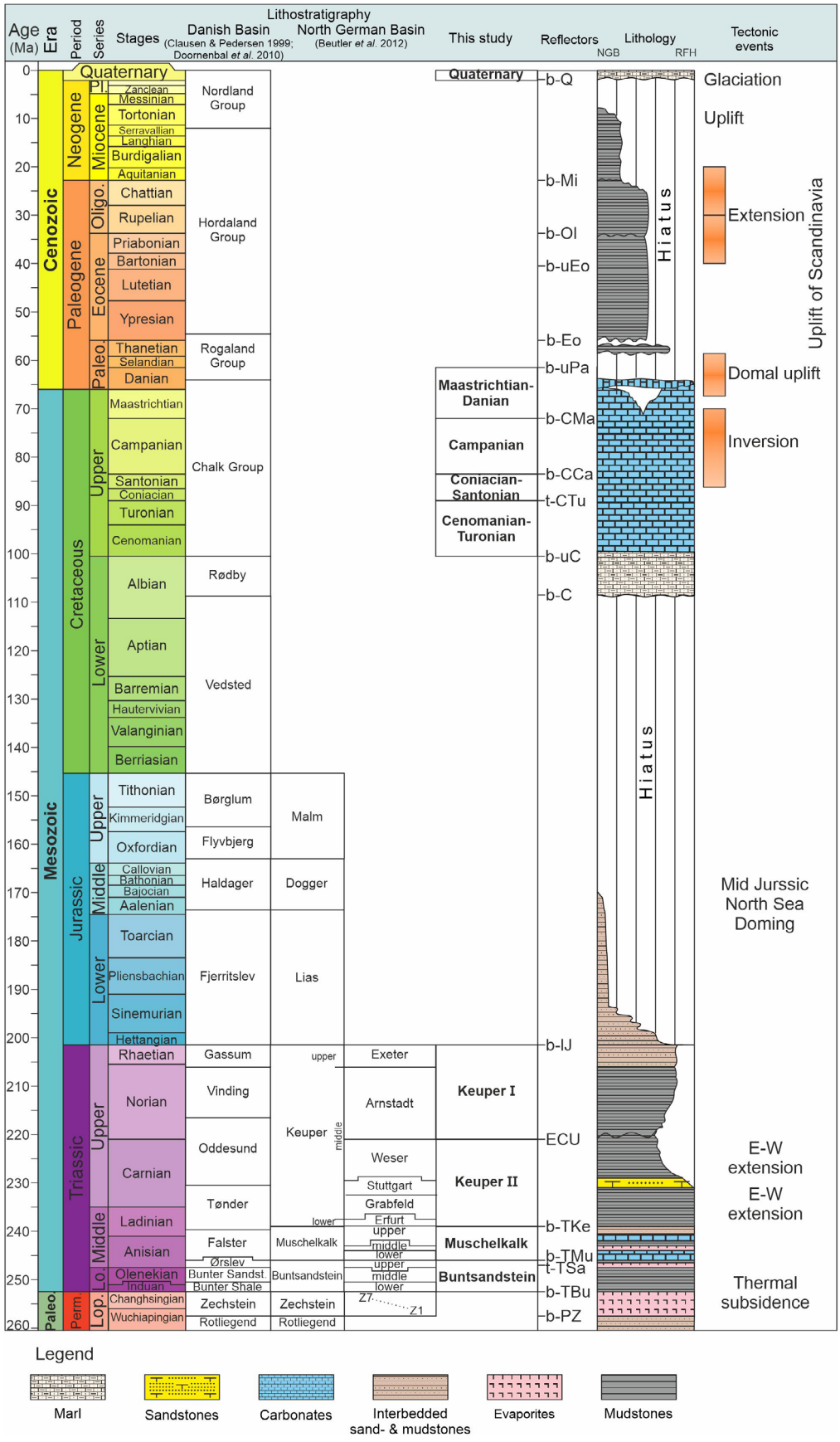
Lithostratigraphy
Age (Ma)
Era
Period
Series
Stages
Danish Basin (Clausen & Pedersen 1999; Doornenbal et al. 2010)
North German Basin (Beutler et al. 2012)
This study
Reflectors
Lithology
NGB
RFH
Tectonic events
Cenozoic
Mesozoic
Paleogene
Neogene
Cretaceous
Jurassic
Triassic
Quaternary
Pl.
Miocene
Oligo.
Eocene
Paleo.
Upper
Lower
Middle
Lo.
Perm.
Zanclean
Messinian
Tortonian
Serravallian
Langhian
Burdigalian
Aquitanian
Chattian
Rupelian
Priabonian
Bartonian
Lutetian
Ypresian
Thanetian
Selandian
Danian
Maastrichtian
Campanian
Santonian
Coniacian
Turonian
Cenomanian
Albian
Aptian
Barremian
Hauterivian
Valanginian
Berriasian
Tithonian
Kimmeridgian
Oxfordian
Callovian
Bathonian
Bajocian
Aalenian
Toarcian
Pliensbachian
Sinemurian
Hettangian
Rhaetian
Norian
Carnian
Ladinian
Anisian
Olenekian
Induan
Changhsingian
Wuchiapingian
Nordland Group
Hordaland Group
Rogaland Group
Chalk Group
Rødby
Vedsted
Børglum
Flyvbjerg
Haldager
Fjerritslev
Malm
Dogger
Lias
Gassum
Vinding
Oddesund
Tønder
Falster
Ørslev
Bunter Sandst.
Bunter Shale
Zechstein
Rotliegend
upper
middle
lower
Keuper
Muschelkalk
Buntsandstein
Zechstein
Rotliegend
Exeter
Arnstadt
Weser
Stuttgart
Grabfeld
Erfurt
upper
middle
lower
upper
middle
lower
Z7
Z1
Quaternary
Maastrichtian-Danian
Campanian
Coniacian-Santonian
Cenomanian-Turonian
Keuper I
Keuper II
Muschelkalk
Buntsandstein
b-Q
b-Mi
b-Ol
b-uEo
b-Eo
b-uPa
b-CMa
b-CCa
t-CTu
b-uC
b-C
b-lJ
ECU
b-TKe
b-TMu
t-TSa
b-TBu
b-PZ
Hiatus
Hiatus
Glaciation
Uplift
Extension
Uplift of Scandinavia
Domal uplift
Inversion
Mid Jurssic North Sea Doming
E-W extension
E-W extension
Thermal subsidence
Legend
Marl
Sandstones
Carbonates
Interbedded sand- & mudstones
Evaporites
Mudstones

Fig. 2. Lithostratigraphic chart of the northern North German Basin and Ringkøbing–Fyn High area (modified after Ahlrichs *et al.* 2021, 2022). Lithostratigraphic subdivision of the Triassic and Jurassic for the Danish Basin after Clausen & Pedersen (1999). Seismic units mapped in this study are also shown. Reflectors: b-Q = base Quaternary Unconformity; b-Mi = base Miocene; b-Ol = base Oligocene; b-uEo = base upper Eocene; b-Eo = base Eocene; b-uPa = base upper Paleocene; b-CMa = base Upper Cretaceous Maastrichtian; b-CCa = base Upper Cretaceous Campanian; t-CTu = top Upper Cretaceous Turonian; b-uC = base Upper Cretaceous; b-C = base Cretaceous; b-lJ = base Lower Jurassic; ECU = Early Cimmerian Unconformity; b-Tke = base Triassic Keuper; b-TMU = base Triassic Muschelkalk; t-TSa = top Triassic Salinarröt; b-TBu = base Triassic Buntsandstein; b-PZ = base Permian Zechstein. Other abbreviations: Bunter Sand. = Bunter Sandstone; Lo. = Lower; Lop. = Lopingian; Oligo. = Oligocene; Paleo. = Paleocene; Pl. = Pleistocene.

data, which were acquired in September 2020, during a cruise organized by the University of Hamburg (Cruise AL545, Hübscher *et al.* 2020) (Fig. 3). The parametric echosounder data were acquired by using the Innomars SES 2000 parametric sub-bottom profiler, which is hull-mounted on RV 'Alkor'. The system generated primary frequencies of about 100 kHz, while the secondary parametric frequency was set to 8 kHz. Vertical resolution depends on water depth and frequency; overall it was below 6 cm (Wunderlich & Müller 2003). For seismic data acquisition, a Mini-GI gun (true GI-mode with a 15 in^3 generator and 30 in^3 injector volume) and a 48-channel streamer with 4 m group spacing were used. The dominant frequency of the data was 250 Hz. The signal penetration is 1 s two-way travel time (TWT). Seismic processing included frequency filtering, amplitude recovery, noise reduction, and surface-related multiple attenuation to remove strong, reverberating multiples caused by the shallow water depth of the Baltic Sea. All seismic profiles were poststack time migrated. The resulting seismic vertical resolution was in the order of 2–5 m assuming a velocity range of 1600 m s^{-1} (Quaternary) to 4200 m s^{-1} (Buntsandstein) (Ahlrichs *et al.* 2021, 2022).

Additionally, we used seismic profiles of the BaltSeis project, surveys Dana99 and Dana00, which were acquired in 1999 and 2000 respectively. The used seismic equipment consisted of a sleeve gun cluster (70 in^3) and a 48-channel streamer with a group spacing of 6.25 m and 300 m total length. The signal penetration was 2 s TWT, and the vertical resolution amounted to 8–10 m (see Hansen *et al.* 2005 for further details). These profiles run from offshore northern Langeland Island southwards into the Bay of Kiel, thus allowing a connection and hence the stratigraphic interpretation of the new data along with previous investigations focused on the Bay of Kiel and Bay of Mecklenburg which were within the scope of the *StrucFlow* and *NeoBaltic* projects (Hübscher *et al.* 2004, 2010; Hansen *et al.* 2007; Al Hseinat *et al.* 2016; Al Hseinat & Hübscher 2017; Ahlrichs *et al.* 2020, 2021, 2022; Frahm *et al.* 2020; Huster *et al.* 2020). Hence, the stratigraphic interpretation in this study followed the seismo-stratigraphic framework developed by Ahlrichs *et al.* (2020, 2021, 2022). Within this framework, the stratigraphic interpretation was based on the integration of seismic and well data from deep research and hydrocarbon exploration wells (Nielsen & Japsen 1991; Hoth *et al.* 1993; see Ahlrichs *et al.* 2020 for a detailed description). The identified reflectors were the base Quaternary Unconformity, base Maastrichtian, base Campanian, top Turonian, base Upper Cretaceous, Early Cimmerian Unconformity, base Keuper, base Muschelkalk, top Salinarröt and base Buntsandstein (Fig. 2).

For mapping, we used all available data to compute two-way travel time structure maps for each seismic horizon by minimum curvature spline interpolation with a grid cell size of 100 × 100 m. By subtraction of the time–structure maps, we calculated isochron maps as an estimation of the thickness of each unit (vertical thickness in TWT). Owing to the lack of seismic depth data and nearby wells with sufficient velocity information, depth conversion is a challenging open task. To get an idea of the imaged depth range, we approximated the depth for each profile and the thickness in metres represented by the isochron maps using a constant velocity approach. The respective velocity is noted in the figure captions. We identified multiple faults on the seismic profiles, which we traced across seismic profiles and included in the maps. Some of the tectonic faults could be correlated with anomalies in the electrical resistivity distribution on Langeland Island (Fig. 3).

Stratigraphic interpretation of the sediment echosounder data was based on previous studies carried out adjacent to our study area (Bennike *et al.* 2004; Bendixen *et al.* 2013; Endler *et al.* 2016). Accordingly, we interpreted structureless deposits, which strongly absorb signal energy as till. High-amplitude, banded parallel reflections, following the morphology of the till, characterize the deposits of the Baltic Ice Lake stage while high-frequency, parallel and conformable reflections are attributed to the Littorina and post-Littorina units (Endler *et al.* 2016). Within the study area, the GEUS earthquake database lists a single earthquake of magnitude 2.3 located in the central part of Langeland Island (Fig. 3) (GEUS seismologi 2022).

Diffraction imaging

To better image and interpret fault systems, we estimated diffraction-energy images (Preine *et al.* 2020). Wave diffraction occurs when the seismic wavefield encounters small-scale scattering objects such as faults, pinch-outs, or erosional surfaces (e.g. Landa & Keydar 1998; Schwarz 2019a). While diffractions are neglected in most state-of-the-art processing and interpretation schemes,

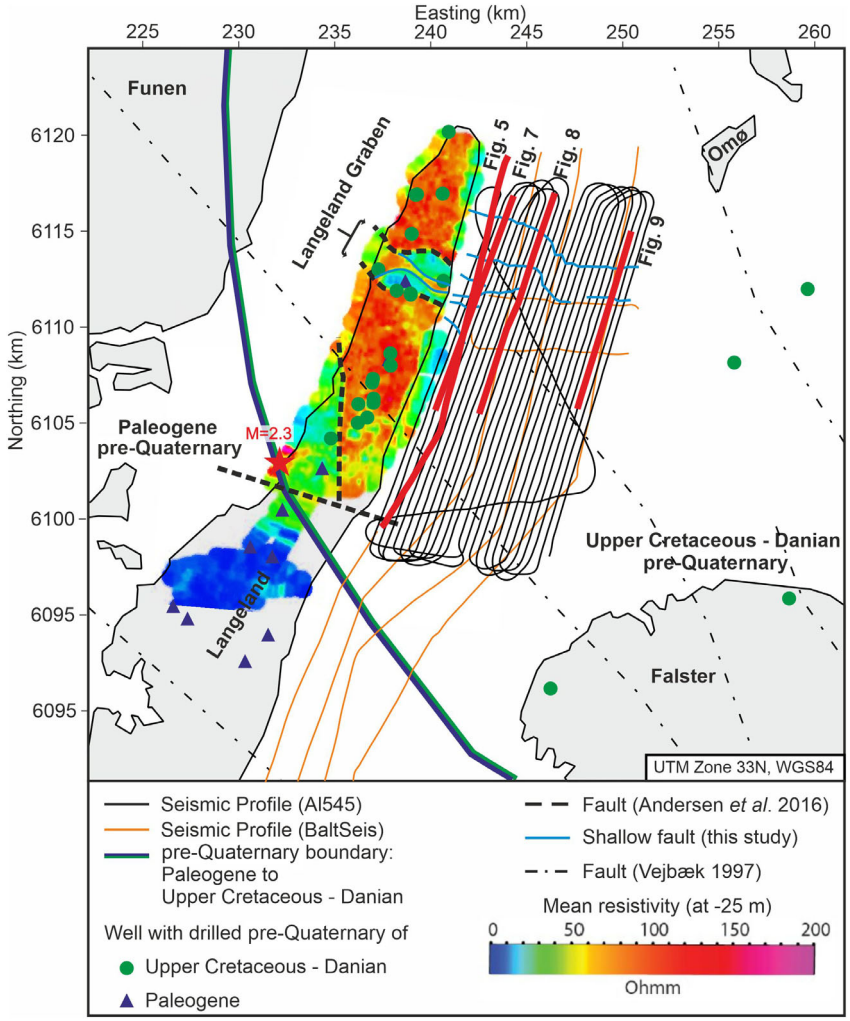

Fig. 3. Seismic database used in this study shown together with shallow wells (obtained from Jupiter well database, Hansen & Pjetursson 2011), major faults (Vejbæk 1997), the dominant pre-Quaternary geology (according to Japsen *et al.* 2007) and mean resistivity at an elevation of 25 m below the surface (airborne electromagnetic data from Andersen *et al.* 2016). Well symbols indicate the pre-Quaternary succession drilled in the well. Red shows the location of an earthquake listed in the GEUS database (magnitude 2.3; GEUS seismologi 2022).

the value of diffraction as a tool for obtaining additional information for processing and interpretating seismic data has become more recognized in recent years (e.g. Preine *et al.* 2020; Schwarz & Krawczyk 2020; Ford *et al.* 2021).

In the present study, we used the diffraction-imaging approach that has been proposed by Preine *et al.* (2020), which consists of the following two steps: diffraction separation and diffraction focusing. In the first step, we separated the diffracted wavefield from the reflected wavefield, using an approach that was introduced by Schwarz & Gajewski 2017 and extended by Schwarz (2019b). This approach first separates the dominant reflected wavefield through a coherent summation scheme guided by a dip-based wavefront filter (Schwarz & Gajewski 2017; Schwarz 2019b). Afterwards, the diffracted wavefield is obtained by subtracting the reflection-only data from the input data (Fig. 4A, B). In the second step, we applied FD Migration to the diffraction-only data to focus the diffractions (Fig. 4C). By calculating the squared envelope of the focused diffractions, we obtained the diffraction energy, which we blended with the time-migrated images (Fig. 4D) (Preine *et al.* 2020). The combination of the conventional full-wavefield image and the diffraction-energy image allowed a better interpretation of the faults and small-scale heterogeneities (Fig. 4E).

Observations

Using key reflection seismic profiles and diffraction images, we analysed the fault system offshore eastern Langeland Island. Thereafter, we interpreted lineaments of increased diffraction energy in the vicinity of the

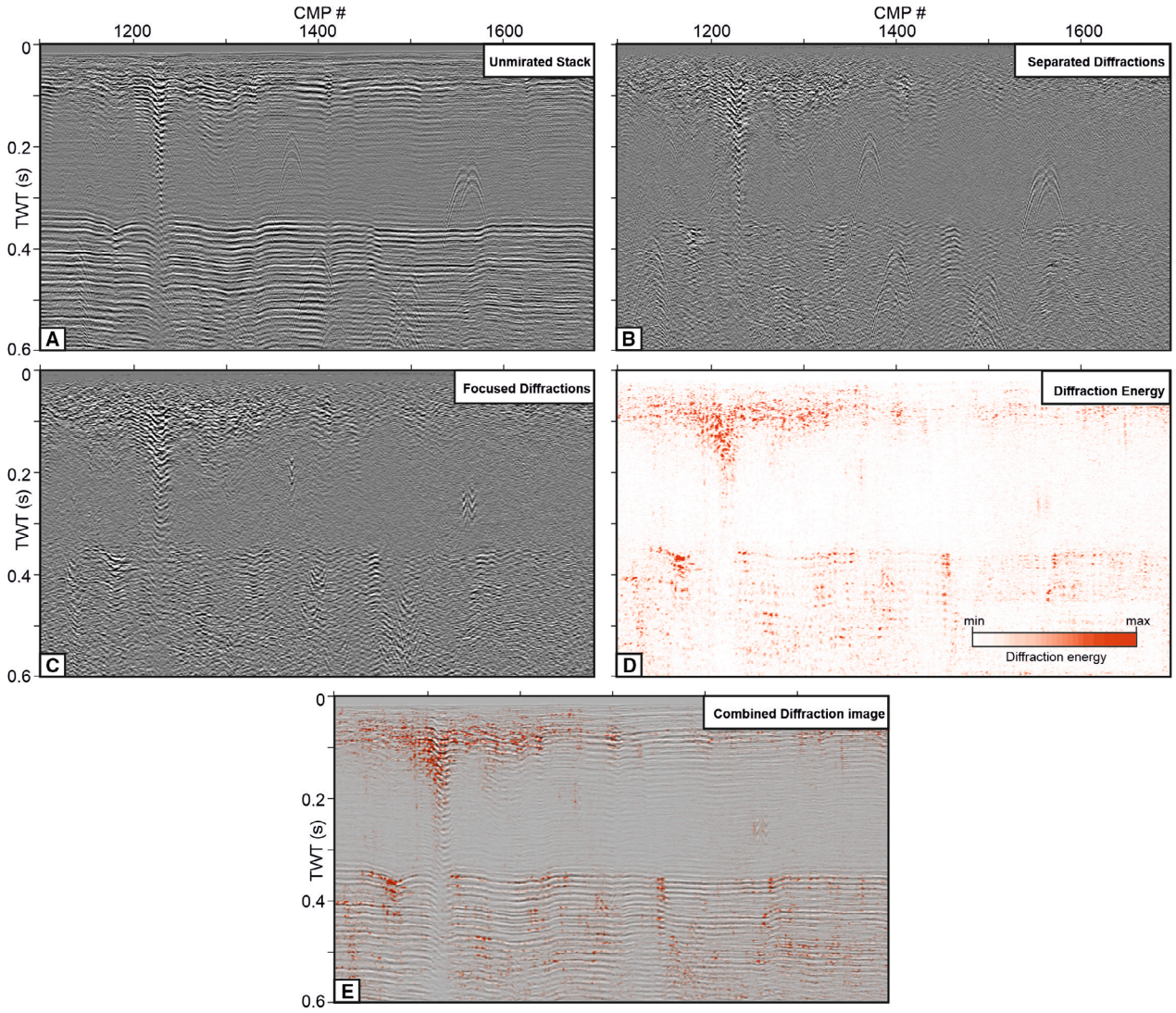

Fig. 4. Diffraction energy estimation scheme. Using an unmigrated stack (A), we first estimated the diffraction-only data (B) before we focused them (C) and estimated the squared envelope to obtain the diffraction energy (D). Blending the full-wavefield migrated image with the diffraction energy helps with the identification of the faults (E).

reflector discontinuities as an indication of the presence of a fault. We used the lineaments as a proxy for fault traces with a focus on identifying shallow faults that were hardly visible on reflection-only data. We considered thickness variations and changea in fault throw within stratigraphic units as indications of vertical motions along the fault and use these observations to analyse the timing of active faulting.

Figure 5 shows a seismic profile located close to the eastern coast of Langeland Island. It illustrates the Triassic to Quaternary subsurface. Between approximately profile kilometres 1 and 6, the reflection pattern in the deeper part of the section is strongly disturbed, and it is not possible to trace any reflections (Fig. 5). In the northern part, various faults are visible, which reach from the Triassic succession up to the base Quaternary. These faults form two major Y-shaped grabens and we will refer to them as the Langeland Fault System (LFS) (Fig. 5, northern graben bound by faults F6 and F7, southern graben by faults F4 and F7). In the central part of the profile, the base of the Triassic deposits is elevated over a zone of approximately 2.5 km (between faults F1 and F2) and we will refer to this area as a basement high and discuss this later in this paper. It is to be noted that the Triassic units dip southward south of the basement high while to the north, the Triassic strata has a northward dip. The Buntsandstein II unit has reduced thickness above the high, while the thickness increases towards the north and southern parts of the profile (Fig. 5). The Buntsandstein I unit is relatively thin across the profile. Slightly increased thickness is visible in the hangingwall of fault F2 and within the graben between the faults F6 and F7, suggesting Early Triassic faulting. The lower part of the Muschelkalk unit shows a divergent pattern above the

basement high when compared with the b-Tke reflector with internal reflections in the unit (dashed line in Fig. 5). The thickness of the Muschelkalk unit increases from the basement high towards the north, which indicates increased relative subsidence. Within the upper part of the Muschelkalk, the divergent pattern becomes less prominent, which could suggest a decrease in subsidence. The overlying Keuper succession is reduced above the basement high and has increased thickness in the south and north (Fig. 5). Only a thinner remnant of the Keuper

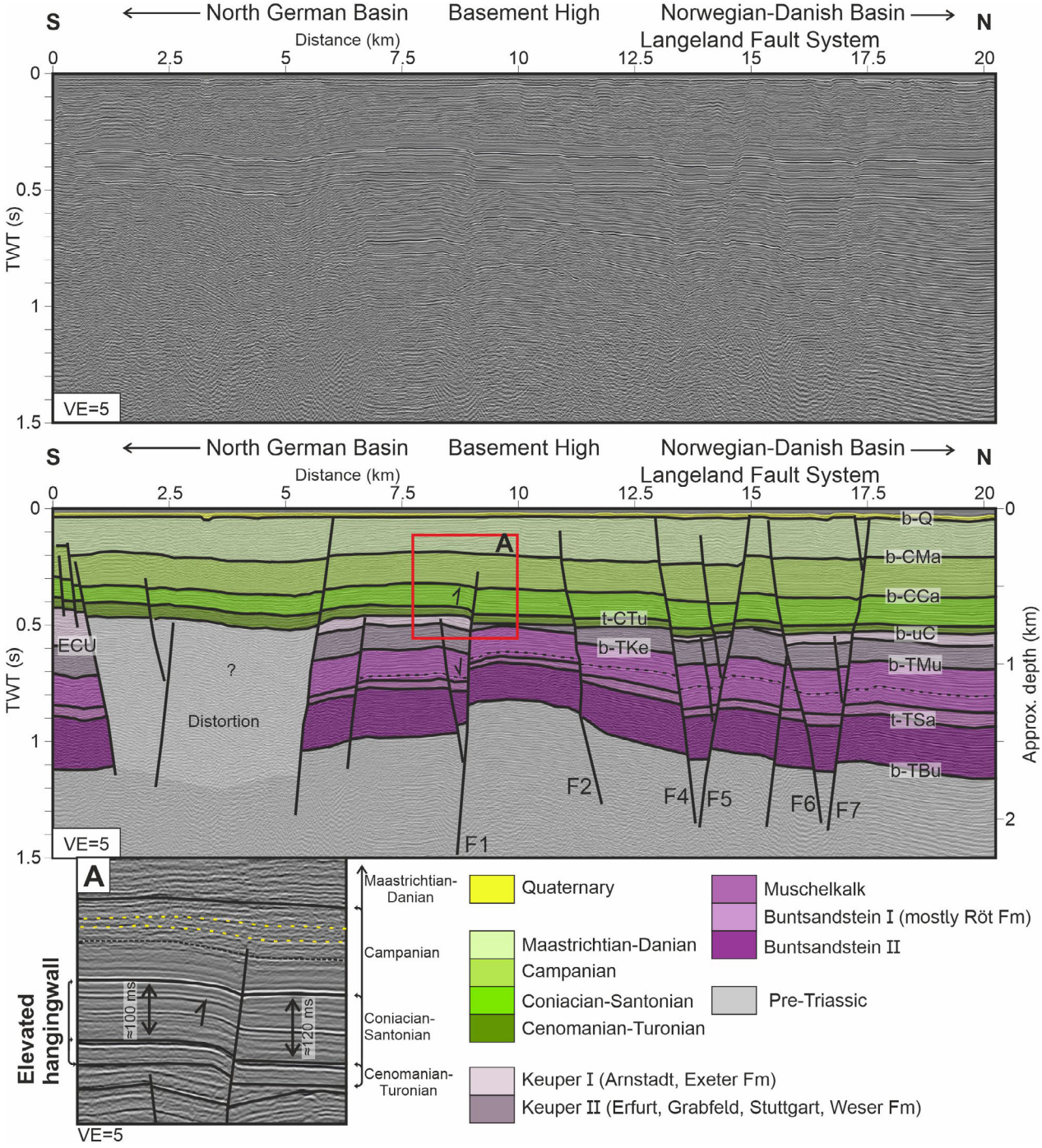

Fig. 5. Profile Dana00-01, located near the east coast of Langeland Island (see Fig. 3 for location). Uninterpreted and interpreted section. Depth was approximated using a constant velocity of 3 km s^{-1}. See Fig. 2 for reflector abbreviations. Kinematic arrows denote inversion of the fault F1. A. Enlarged section as highlighted by the red box. Yellow dashed lines indicate convergent reflectors. Fm. = Formation; VE = vertical exaggeration.

II unit is preserved above the basement high owing to erosion, causing the base Upper Cretaceous unconformity. Keuper I deposits are only preserved within the grabens of the LFS and further north as well as south of the fault F1 (Fig. 5).

The overlying Upper Cretaceous units show a relatively horizontal layering (Fig. 5). The Cenomanian–Turonian unit has a uniform thickness. For the Cenomanian–Turonian and Coniacian–Santonian units, the hangingwall of the fault F1 is elevated above the footwall (Fig. 5), which indicates a reactivation of this Triassic normal fault as a reverse fault during the Late Cretaceous. Inversion began during the Coniacian–Santonian, which is evident in the reduced thickness of the uplifted hangingwall (Fig. 5A). The lower part of the Campanian unit also shows indications of reverse faulting as evidenced by the reduced thickness of the uplifted hangingwall (Fig. 5A). Within the upper part of the Campanian unit, this pattern decreases in intensity and reflections drape on the hangingwall (Fig. 5; yellow dashed lines in Fig. 5A). Within the LFS, the Coniacian–Santonian units are relatively uniform in thickness. Slightly increased thickness within the northern graben (F6 and F7) could suggest active faulting during the Campanian (Fig. 5). Within the Maastrichtian–Danian unit, fault throw along the fault F4 increases alongside the increased thickness within the graben (F4 and F5). This indicates a reactivation of the LFS during the Maastrichtian. All major faults of the LFS reach up close to or into the Quaternary and eventually pierce the sea floor, which could suggest a possible glacial or post-glacial fault reactivation (Fig. 5).

Spatial pattern of the Langeland Fault System

Fault analysis across all available profiles reveals the spatial pattern of the LFS. Time–structure maps of the base Muschelkalk and top Turonian reflectors in combination with three profiles covering the western, central and eastern part of our study area present the outline and spatial differences of the LFS (Figs 6–9). Figures 7–9 show the time-migrated seismic images blended with the diffraction energy (top) and the final interpreted time-migrated sections (bottom).

Fault F1 is an approximately east–west oriented normal fault marking the southern border of the local basement high, which causes a visible local high in the base Muschelkalk time–structure map (Fig. 6A). The high is more prominent in the western part of our study area and becomes deeper buried towards the east. In combination with an antithetic fault to the south, the fault F1 forms a Y-shaped Triassic graben (Fig. 6A) with fault traces well visible as lineaments of increased diffraction energy (Figs 7–9). The graben was inverted during the Coniacian–Santonian and Campanian as indicated by the uplifted hangingwall of the fault F1, decreased thickness of the Coniacian–Santonian unit and draping in the upper Campanian unit (Figs 6B–9). Fault F2 strikes WNW–ESE along the northern flank of the basement high (Fig. 6A). Within the western study area, fault F2 dissects the entire section from the Triassic to Quaternary (Fig. 7). In the central part, faulting is confined to the Triassic units, whereas further east, fault F2 could not be traced and seems to terminate (Figs 8, 9).

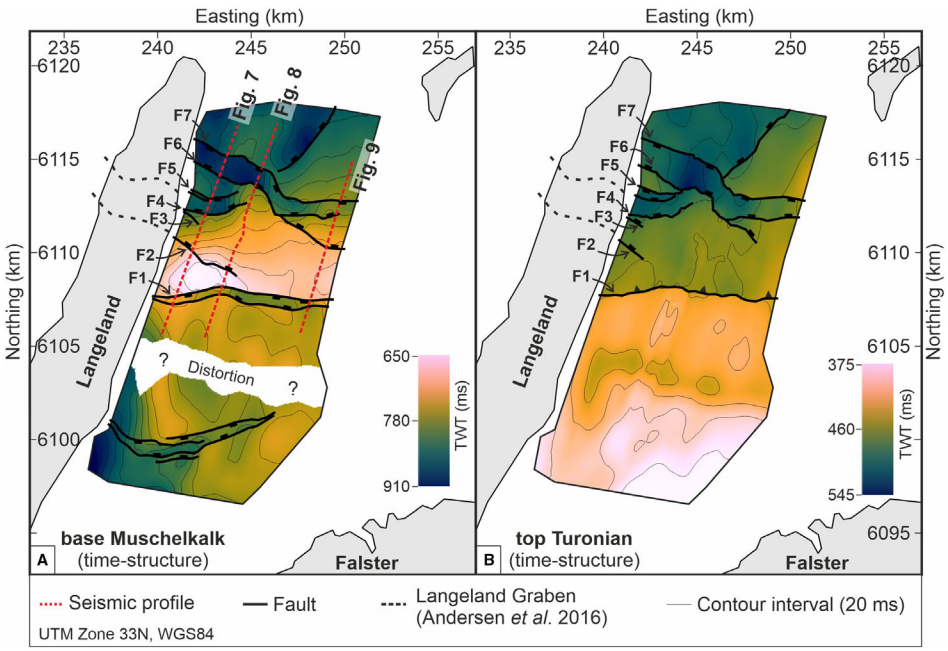

Fig. 6. Base Muschelkalk time–structure map (A) and top Turonian time–structure map (B). Note the change of direction of the fault throw of fault F1 between A and B indicating Late Cretaceous inversion.

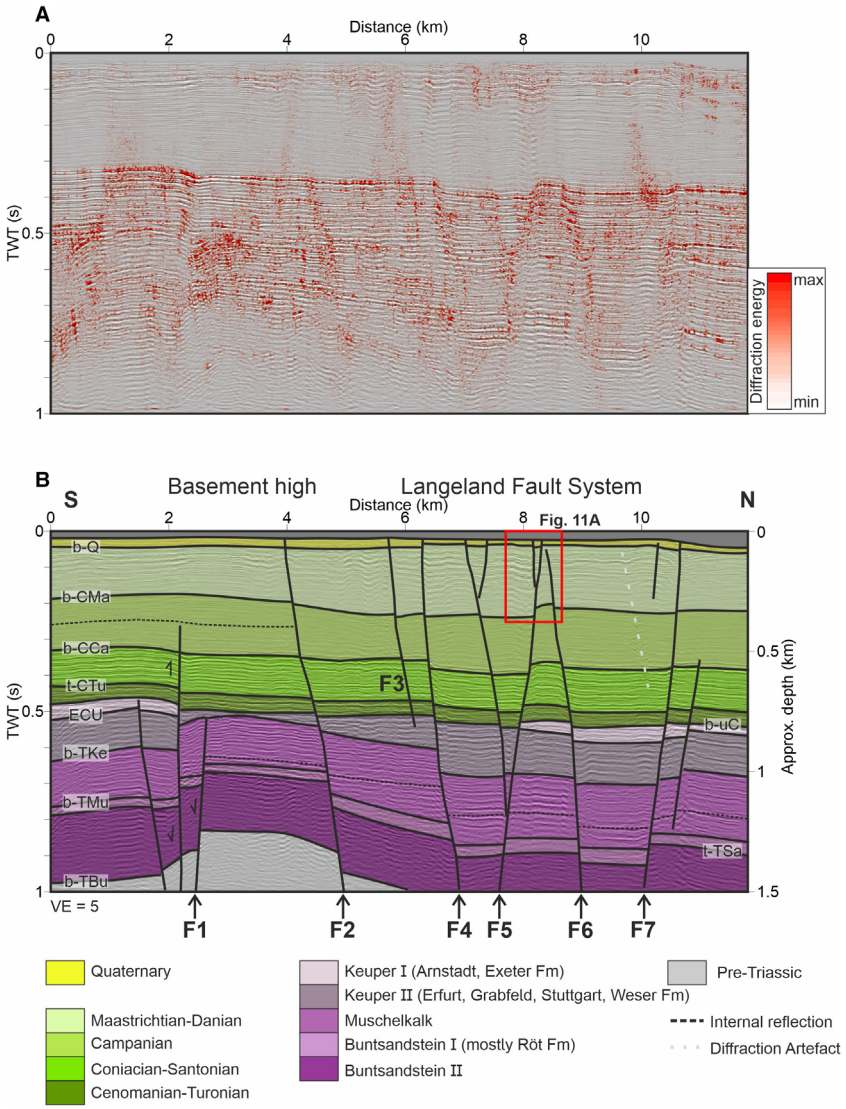

Fig. 7. Profile P40, located near the east coast of Langeland Island (see Fig. 3). A. Time-migrated reflection image blended with diffraction energy from diffraction separation. B. Interpreted time-migrated section. Depth was approximated using a constant velocity of 3 km s^{-1}. Black dashed line mark internal reflections from Muschelkalk and Campanian unit discussed in the text. Grey dashed line indicates a diffraction artefact, probably caused by diffractions originating from ships. See Fig. 2 for reflector abbreviations. Fm. = Formation; VE = vertical exaggeration.

Figure 6 reveals the outline of the two major grabens of the LFS. The graben system consists of a southern branch bound by the faults F4 and F5 and a northern branch bound by the faults F6 and F7 (Fig. 6). The grabens strike approximately WNW–ESE, whereas the southern graben bends towards the north in the central part of our study area and joins the northern graben (Fig. 6). Overall, the western part of the LFS is more faulted, while the eastern part has only two major faults bounding the graben (Figs 6–9).

As observed for Fig. 5, the Muschelkalk unit shows a divergent pattern when comparing the base Muschelkalk reflector (b-TMu) and internal reflections (dashed line in Figs 7–9). Thickness of the unit is reduced above the basement high and increases northwards. This indicates relatively higher subsidence north of the basement high at least in Middle Triassic times. In both grabens, the Keuper II unit shows an increase in thickness, and the bounding faults show decreasing fault throw (Figs 7–9, e.g. F4, F7). Remnants of the Keuper I unit are preserved within the northern graben and the western and central profiles show increased thickness of the graben fill when compared with the graben shoulders (Figs 7, 8). The thickness of the Cenomanian–Turonian, Coniacian–Santonian and Campanian units are relatively uniform across the LFS, which suggests that the grabens were not inverted, and thus, we interpret this as a phase of relative tectonic quiescence (Figs 7–9). The Maastrichtian–Danian unit has increased thickness within both grabens indicating

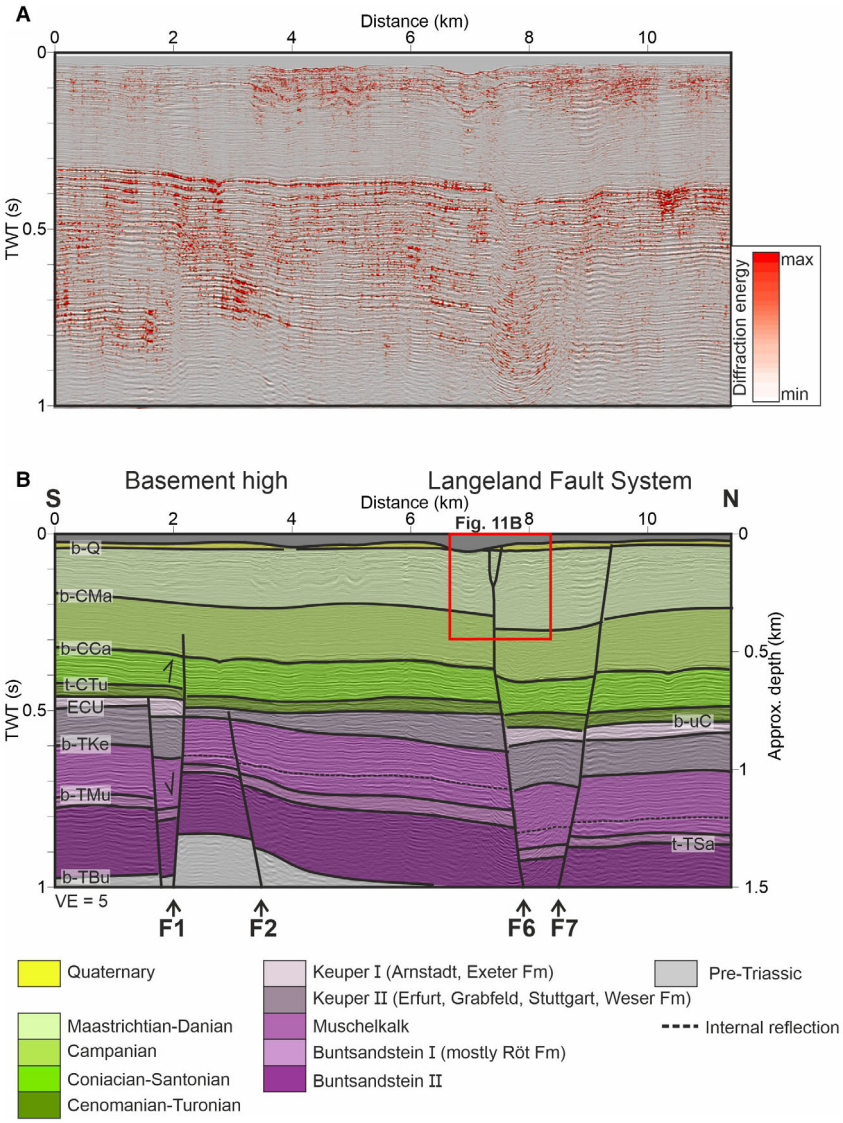

Fig. 8. Profile P41 located in the central part of our study area (see Fig. 3). A. Time-migrated reflection image with blended diffraction energy from diffraction separation. B. Interpreted time-migrated section. Depth was approximated using a constant velocity of 3 km s^{-1}. Black dashed line mark internal reflections from Muschelkalk unit discussed in the text. See Fig. 2 for reflector abbreviations. Fm. = Formation; VE = vertical exaggeration.

syndepositional fault reactivation and graben subsidence (Figs 7–9).

The Quaternary

The Quaternary succession is relatively shallow and thin across our study area (on average 5–25 ms TWT in thickness, ~4–20 m assuming an average velocity of 1600 m s^{-1}) with an area of slightly increased thickness in the SW (Fig. 10). The base Quaternary time–structure map shows several local depressions and areas where the unit is completely absent (Fig. 10A). These zones correlate with channel-like bathymetric lows, which strike approximately north–south and we interpret them as incised palaeochannels (Fig. 10B). Areas with locally increased thickness of the Quaternary unit are interpreted as valley structures (Fig. 10C). Lithological information from shallow wells onshore Langeland Island indicates that the Quaternary succession consists mostly of glacial deposits and meltwater deposits like sand and clay (Fig. 10D). In the seismic sections, major faults of the LFS pierce the entire imaged record from the Triassic successions up to the base Quaternary and seem to also dissect the Quaternary unit itself; however, the minor thickness and limited seismic resolution hampers a precise fault analysis for the Quaternary (Figs 5, 7–9; faults F4 to F7). In the shallow part, fault F4 forms a shallow Y-shaped graben together with a smaller

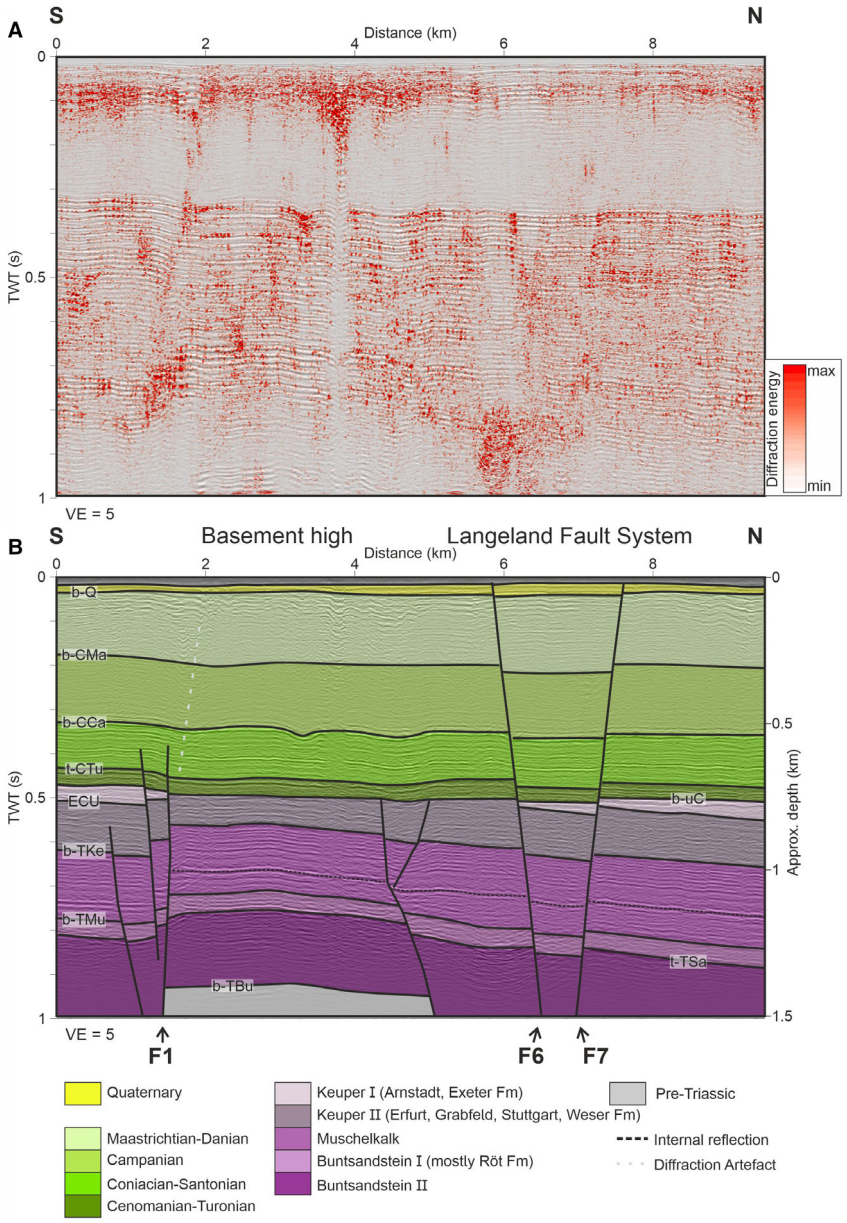

Fig. 9. Profile P26 located in the eastern part of our study area (see Fig. 3). A. Time-migrated reflection image with blended diffraction energy from diffraction separation. B. Interpreted time-migrated section. Depth was approximated using a constant velocity of 3 km s^{-1}. Black dashed line mark internal reflections from Muschelkalk unit discussed in the text. See Fig. 2 for reflector abbreviations. Fm. = Formation; VE = vertical exaggeration.

southward-dipping, antithetic fault (Fig. 7). Figure 11A–C presents enlargements of these features, showing the interpreted reflection image (11B), the reflection image with blended diffraction energy (11C) and the corresponding sediment echosounder image of the faulted area (11A). There are noticeable diffraction energy clusters along sea floor multiple reflections, which represent a form of artefact during the diffraction separation process (white dashed lines in Fig. 11B). Likewise, diffraction energy is sensible to shallow gas effects that are visible by vertical lineaments of diffraction energy, blended above distortions within the reflection image owing to velocity effects (VA in Fig. 11B). For the master fault F4, in Fig. 11B, C, a lineament of diffraction energy can be traced from the deeper subsurface up to the sea floor reflector. A lineament of increased diffraction energy branching of the master fault F4 is interpreted as an antithetic fault. Fault displacement of the base Quaternary reflector is ~4 ms TWT, representing ~3 m assuming a velocity of 1600 m s^{-1} for the Quaternary. The sediment echosounder data show the uppermost ~40 ms deep strata at the assumed position

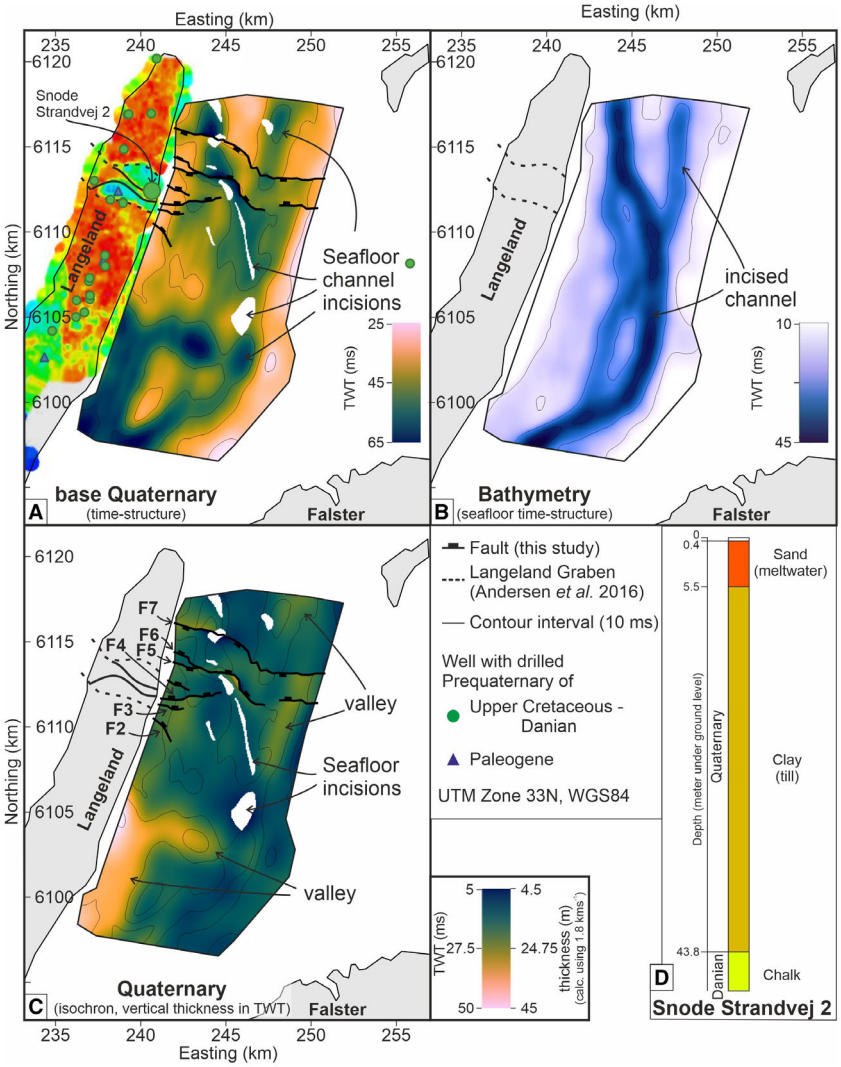

Fig. 10. Base Quaternary time–structure map (offshore) and onshore mean resistivity at an elevation of 25 m below the surface (airborne electromagnetic data from Andersen *et al.* (2016), see Fig. 3 for colour scale) (A), bathymetry represented by the sea floor time–structure map (B) and Quaternary isochron (vertical thickness in two-way travel time) map (C). The contour interval is 10 ms. All maps are in UTM Zone 33 N, WGS84. Shallow wells were obtained from the Jupiter well database (GEUS 2014). The well symbols indicate Prequaternary succession drilled in the well. Exemplary Quaternary lithology is shown for well Snode Strandvej 2 (DGU no. 165.517) (D), see (A) for well location.

indicated by the seismic data (Fig. 11A and spatial correlation to seismic data as indicated by the dotted line). A high-amplitude reflection characterizes the sea floor and directly below lies a well-stratified, high-amplitude unit (Unit 1 in Fig. 11A). A relatively high-amplitude reflector separates Unit 1 from the underlying less stratified Unit 2 with low-amplitude reflections (yellow dashed line). This basal reflector shows several discontinuities with vertical offsets of ~2.5 ms TWT, which we interpret as faulting and the formation of a shallow Y-shaped graben with the northern fault as the shallow prolongation of the F4 master fault (Fig. 11A).

A similar feature is visible for the fault F6, which likewise forms a shallow Y-shaped graben (Fig. 8). As above, Fig. 11D–F shows the interpreted reflection image together with the blended diffraction energy and the corresponding sediment echosounder data. Likewise, diffraction energy clearly clusters along the sea floor multiples, representing an artefact in the diffraction separation process (white dashed lines in Fig. 11E). Master fault F6 is clearly visible as a lineament of increased diffraction energy (Fig. 11E, F). Within the uppermost 100 ms TWT, the strata is strongly faulted and fault throw is clearly visible at the base Quaternary reflector (b-Q) (~4.2 ms TWT representing ~3.4 m assuming 1600 ms^{-1} for the Quaternary) (Fig. 11E). Lineaments of increased diffraction energy mark the fault traces of the fault F6 and a southward-dipping, smaller antithetic fault (Fig. 11E, F). Thereby, the graben is located at the northern flank of the channel incised into

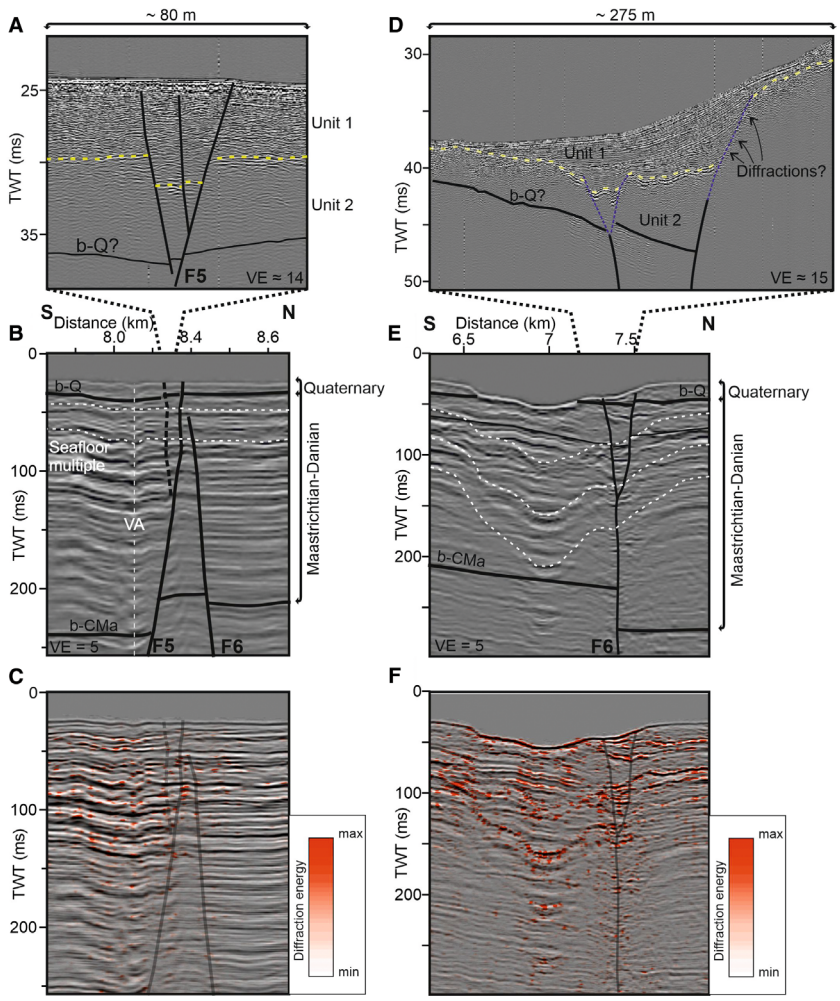

Fig. 11. Enlargements of seismic reflection images, diffraction energy and sediment echosounder data. A. Sediment echosounder section above Fault F4, dashed grey line shows spatial extend in seismic data below. B. Interpreted seismic reflection image corresponding to the red rectangle in the section in Fig. 7. C. Reflection image with blended in diffraction energy. D. Sediment echosounder data above Fault F6, dashed grey line shows spatial extent in seismic data below. E. Interpreted seismic reflection image corresponding to the red rectangle in Fig. 8. F. Reflection image with blended diffraction energy. Note the clustering of diffraction energy along faults and sea floor multiples (white dashed lines). VA= Velocity artefact; VE = vertical exaggeration.

the sea floor (see Fig. 10B). The corresponding sediment echosounder image shows the uppermost 50 ms TWT at the assumed position of the master fault F6 (Fig. 11D). The sea floor is characterized by a high-amplitude reflector, which dips towards the south owing to the position within the channel. The sediment echosounder image shows a well-stratified depression with high-amplitude reflections that wedge out towards the south (Unit 1). At the northern end, the base of Unit 1 shows a distinct offset of ~6 ms TWT (Fig. 11D, yellow dashed line). Here, reflections terminate sharply and the reflection pattern shows hyperbola-like features, which resemble diffractions (blue dashed line, Fig. 11D). Further discontinuities at the basal reflector are visible in the central part of the image (yellow dashed line, Fig. 11D). These discontinuities correlate with the position of the Y-shaped graben, observed in the seismic data, and could be interpreted as the shallow prolongation of the master fault F6.

A comparison between the seismically mappable faults with the approximately west–east-striking lineations in the electrical resistivity distribution on Langeland Island shows only limited correlation. The Langeland Graben as identified by Andersen *et al.* (2016) lies to the west only of the southern LFS. Resistivity lineations within the trench lie west of fault F4 (Fig. 10).

Interpretation and discussion

The Langeland Fault System within the structural framework

The presence of conjugate normal faults rooted within the Pre-Triassic, which dissect the Triassic to Quaternary

successions and form a graben offshore the northern east coast of Langeland Island, is already known (Al Hseinat & Hübscher 2017). Seismic imaging and fault analysis in this study revealed that the previously discovered faults are part of a larger WNW–ESE-striking fault system consisting of several faults, forming two major grabens, which we refer to as the LFS (Fig. 6). In the central part of our study area, the southern graben bends towards the north and joins the northern graben. Thereby, the southern graben forms the offshore prolongation of a shallow graben observed in airborne electromagnetic data onshore Langeland Island (Andersen *et al*. 2016). The postulated layer of the Paleocene sediments within the graben could not be identified on our seismic data; however, this layer might be too thin to be resolved. South of the LFS, we identified a ~east–west-striking fault, which dissects the entire Triassic subsurface and reaches into the Pre-Triassic successions (F1). This fault forms the southern border of a block of elevated Triassic strata, whose location coincides with an east–west continuation of the Glamsbjerg High, where the basement is directly underlying the top Pre-Zechstein (Vejbæk 1997) (Figs 1, 6A). This bounding fault was imaged by a recently published industry seismic profile showing the elevated top Pre-Zechstein and elevated overlying Triassic units north of the fault (Ahlrichs *et al*. 2022: fig. 7). Additionally, it is visible that the fault pierces the thin Zechstein unit and is rooted within the Pre-Zechstein subsurface. Therefore, we interpret the elevated Triassic strata observed in our data as an expression of elevated basement related to the Glamsbjerg High. Accordingly, this area is part of the RFH and marks the transition between the North German and Norwegian–Danish basins (Fig. 1). Towards the eastern part of our study area, the Triassic strata are less elevated, which suggests that this part covers the margin of the basement high (Fig. 9). Investigations from the North Sea sector of the RFH suggested that WNW–ESE-trending fracture zones form the border of the RFH; however, a fault-limited RFH was questioned based on seismic investigations in the central part of the RFH (Cartwright 1990; Clausen & Pedersen 1999). At least within our study area, our seismic data prove that the southern border of the high is fault bounded (fault F1 in Figs 5–9).

The reduced thickness of the Buntsandstein unit above the basement high and the increasing thickness towards the north and south indicate differential subsidence and the presence of the high during deposition (Fig. 5). This differential subsidence continued during deposition of the Muschelkalk expressed by reduced thickness above the basement high and gradually increasing thickness away from it (Figs 5–9). This is in accordance with the Early to Middle Triassic thermal subsidence of the North German and Norwegian–Danish basins and the concept of relatively slower subsidence along the RFH (Clausen & Pedersen 1999; Sachse & Littke 2016). The imaged Keuper units are strongly affected by erosion related to Mid Jurassic uplift of the RFH (Michelsen 1978; Bertelsen 1980). The fault array and spatial distribution resembles the top part of a negative flower structure (especially Figs 5 and 7, compare, e.g., with Huang & Liu 2017), which could represent a Late Triassic reactivation of preexisting basement faults, which developed by late Carboniferous–early Permian dextral strike-slip movements during the initial development of the RFH (EUGENO-S Working Group 1988; Thybo 1997; Vejbæk 1997).

The Late Cretaceous fault reactivation

The uniform thickness of the Cenomanian–Turonian unit suggests a phase of relative tectonic quiescence without faulting which is in accordance with observations within the Baltic sector of the North German Basin, to the south of our study area (Figs 5, 7–9) (Ahlrichs *et al*. 2021). The inversion of the fault F2 at the southern flank of the basement high during the Coniacian–Santonian and Campanian is in agreement with the timing of adjacent inversion structures and the onset of Africa–Iberia–Europe convergence inducing compressional stress within the European foreland (Figs 5–9) (Vejbæk & Andersen 2002; Krzywiec 2006; Kley & Voigt 2008; Kley 2018; Ahlrichs *et al*. 2021). Contrarily, the faults of the LFS do not show indications of inversion, as the Coniacian–Santonian and Campanian units are relatively uniform in thickness (Figs 5, 7–9). Rather, the increased thickness of the Maastrichtian–Danian unit within the grabens of the LFS suggests normal fault reactivation during this time (Figs 5, 7–9). Why the fault at the southern flank of the basement high was reactivated during Late Cretaceous inversion (Conicaian–Campanian) but the faults of the LFS were not, despite the similar and favourable alignment for north–south-acting shortening, remains ambiguous. A possible explanation might be that the impact of Late Cretaceous compression localized across former structural boundaries (Rasmussen 2009) and thus, the basement high might have shielded the LSF from compression from the south.

The Quaternary faulting within the Langeland Fault System

The outline of the channel structures visible within the bathymetry is in accordance with the postulated paleochannel of the Dana River, which developed as a drainage pathway from the Bay of Mecklenburg via the Langeland Belt into the Storebælt during the Ancylus Lake stage (9.2 ka BP; Fig. 10B) (Winn 1974; Björk 1995).

Faults visible within the seismic data could be traced from the Mesozoic subsurface up to the base Quaternary reflector and seem to propagate across the Quaternary successions up to the sea floor (Figs 5 and 7–9). This suggests a Quaternary fault reactivation and was previ-

ously explained by stress induced from ice sheet loading in combination with the present-day stress field (Al Hseinat & Hübscher 2017). In this study, fault analysis, supported by the overlay of separated diffraction energy, revealed the spatial pattern of the LFS showing that faults displace the Quaternary succession and reach up to the sea floor across the entire graben system (Figs 5 and 7–10). This implies a Quaternary fault reactivation across the entire analysed LFS, that is, over a length scale of a minimum 8.5 km. The uppermost succession imaged by the sediment echosounder data further supports a Quaternary fault reactivation of the LFS (Fig. 11). Displacements of reflectors within the unconsolidated sediments suggest postdepositional faulting. These displacements are in the prolongation of projected faults visible within the seismic data, which implies that faults identified in seismic data propagate across the Quaternary up to the sea floor (Fig. 11). Well information from Langeland Island shows that the Quaternary succession consists exclusively of glacial and postglacial deposits (Fig. 10D). In any case, visible faulting affects these deposits, thus indicating fault reactivation either in glacial or in postglacial times.

The cause of the only limited lateral correlation between the LFS and the electrically mappable structures of the Langeland Graben is contentious. For example, it should be considered that electrical resistivity depends primarily on the properties of the pore space fluids, which in turn are controlled by porosity (e.g. Bhattacharya & Patra 1968). The spatial grain size thus plays a greater role in the electromagentic data than in the seismic images.

The cause for Quaternary fault reactivation of the Langeland Fault System

In principle, two possible causes for the Quaternary fault reactivation seem to be the most valid: either glacially induced faulting, thus, fault reactivation by stress originating from glacial isostatic adjustments, or by stress from the regional tectonic stress field, thus, originating from plate or intraplate tectonics. Owing to the temporal correlation, glacially induced faulting caused by stress from glacial isostatic adjustments seems to be the obvious explanation for fault reactivation across the LFS. Notably, the WNW–ESE orientation of the LFS with fault displacements of a few metres is in accordance with the other postulated glacially induced structures in Denmark (e.g. reactivated faults of the Sorgenfrei–Tornquist Zone (Børglum Fault), near Nørre Lyngby: Lykke-Andersen 1992; Brandes *et al*. 2018, 2022; Tønder Graben: Sandersen & Jørgensen 2015; see Sandersen *et al*. 2021 for an overview of glacially induced faulting in Denmark). For instance, neotectonic activity at the Børglum Fault caused soft-sediment deformation structures and normal faulting in the late glacial sediments with fault displacements ranging from a few centimetres up to 3 m. On the Danish mainland near Brande, glacially induced fault movements are explained by a reactivation of older NW–SE dextral strike-slip faults along the northern flank of the RFH (Lykke-Andersen *et al*. 1996). These similarities in orientation, fault displacement and context of the structural framework support the interpretation of glacially induced fault reactivation of the LFS. The evaluation of recently detected deep crustal earthquakes in northern Germany showed a correlation with the deep-reaching part of the Caledonian Deformation Front, which is located south of the LFS (Fig. 1) (Brandes *et al*. 2019). Based on numerical modelling, the authors concluded that stress changes owing to glacial isostatic adjustments most likely triggered these earthquakes. In the Bay of Kiel and Pomeranian Bay, Al Hseinat & Hübscher (2017) interpreted Quaternary fault reactivation of Mesozoic–Cenozoic fault systems, some of which were re-evaluated by Frahm *et al*. (2020). The recent fault reactivation was related to glacially induced stress acting in combination with the present-day stress field and thus, agree with observations along the LFS.

In general, modelling results suggest that stress from glacial isostatic adjustments can reactivate pre-existing faults in a thrust, strike-slip or normal stress regime and indicate that reactivation is largely dependent on the location of the fault to the ice sheet and the current stress ratio (Steffen & Steffen 2021). During the maximum extent of all three major Pleistocene glaciations, our study area was fully covered by ice sheets (e.g. Hughes *et al*. 2016). Consequently, over time, the faults of the LFS were affected by different stresses during the ice advance and retreat, covering the full range of locations relative to the ice masses from fully covered by the ice sheets, to ice margin area and the peripheral bulge (e.g. Steffen *et al*. 2021b). The offset of Quaternary reflectors by fault F4 and related antithetic faults forming a Y-shaped graben (Fig. 11A) indicate normal fault reactivation. Likewise, normal fault reactivation of the fault F6 and the formation of a shallow Y-shaped graben could explain the development of the valley with increased thickness of presumably postglacial Littorina sediments (Unit 1 in Fig. 11). However, a valley formation by coincidental glacial erosion above the fault cannot be excluded and further mapping of this structure needs to verify the spatial correlation of valley and subsurface fault. Accordingly, glacially induced faulting within the LFS seems plausible. However, future studies should refine the timing of Quaternary fault reactivation in correlation with the timing of ice advance or retreat and the location of the ice sheets with respect to the faults to verify faulting induced by glacial isostatic adjustments.

Whether the Quaternary fault reactivation of the LFS could have been caused by plate or intraplate tectonics unrelated to the glaciations depends on the orientation and character of the present-day stress field. The present-day stress field has an NW–SE to north–south direction within central Europe and is thought to have been almost

stable since the Oligocene (Kley *et al*. 2008). For northern Germany and Denmark, the smoothed global intra-plate stress of the World Stress Map shows north–south-directed mean maximum horizontal stress S_{HMAX} (Heidbach *et al*. 2018), which would be a more favourable orientation for a reactivation of the almost east–west-oriented faults of the LFS. However, besides borehole breakout data records near Als Island showing NW–SE-directed maximum horizontal stress and onshore Mecklenburg–Western Pomerania showing NNW–SSE stress, further data records in the southwestern Baltic Sea are absent. Hence, the true present-day stress field near Langeland Island remains ambiguous. However, it is possibly in the range of NW–SE to NNW–SSE maximum horizontal stress. Modelling results showed that a strike-slip to reverse faulting regime is present in the uppermost subsurface, which dominantly becomes a normal faulting regime with depth (Ahlers *et al*. 2021). From the orientation of the present-day stress field, a recent reactivation of the LFS cannot be excluded. Mobile Zechstein salt is absent below the LFS, hence, detached faulting is unlikely (see limit of mobile Zechstein in e.g. Ahlrichs *et al*. 2021). Indications of thrust faulting are lacking in the sediment echosounder data (Fig. 11).

Therefore, a glacial or postglacial reactivation may stem from stress induced by glacial isostatic adjustments in combination with the present-day stress field as denoted by Al Hseinat & Hübscher (2017). However, postglacial uplift and re-adjustments of the lithosphere are thought to significantly influence the regional stress field, suggesting significant glacially induced control on fault reactivation (Sirocko *et al*. 2008; Steffen *et al*. 2021a). For the LFS, future studies improving the mapping of the fault system and onshore prolongation in combination with different approaches, e.g. by using LiDAR data to reveal small-scale topography changes in the vicinity of faults and studies modelling the glacially induced stress on the faults, should shed light on recent or ongoing fault reactivation and the general reactivation potential of fault systems affected by glacial isostatic adjustment stress.

Geophysical identification and quantification of the Quaternary reactivation of nearby faults

As outlined earlier, there is ample evidence for Quaternary fault activity in northern Europe. However, there are few studies that clearly image and demonstrate the relationship between shallow and inherited faults through geophysical data. In this study, reflection seismic data imaging the subsurface from the sea floor down to the Triassic were combined with parametric sediment echosounder data to achieve this goal.

A similar approach was carried out for the Carlsberg Fault south of Copenhagen. Here, the combination of terrestrial high-resolution shear-wave vibrator seismic profiles in combination with marine reflection seismic data from the offshore prolongation of this fault proved syn-sedimentary tectonic phases from the Triassic to Quaternary (Kammann *et al*. 2016). The shear-wave seismic data imaged shallow normal faults that dissect Quaternary till layers and Danian chalk, backed by the marine data imaging the Triassic to Danian strata. Fault displacements at the base Quaternary are between 5 and 18 m and are, therefore, slightly greater than the observations made in the LFS. The exact timing of the Quaternary reactivation of the Carlsberg Fault remains unclear; however, the authors suggest a Late Pleistocene activity, even though other causes apart from neotectonics may be present (Kammann *et al*. 2016). Notably, the Carlsberg Fault Zone strikes almost NW–SE and thus, has a different orientation than the east–west-striking LFS. However, this does not necessarily contradict a glacially induced reactivation of both fault systems as recent modelling results have shown that faults do not have to be optimally oriented to be reactivated by glacially induced stress (Steffen & Steffen 2021).

The combination of terrestrial high-resolution p-wave vibrator seismics with parametric echosounder, sparker and airgun seismics imaged Quaternary fault reactivation of a crestal graben structure above a salt wall in the western Bay of Kiel (Al Hseinat *et al*. 2016). As later supported by Huster *et al*. (2020), the fault reactivation was associated with stress induced from ice-sheet loading and unloading. Visible depressions in sediment echosounder data above the faults filled with increased thicknesses of presumably postglacial Littorina sediments (Fig. 11 in Huster *et al*. 2020) are similar to the observations from the shallow subsurface of fault F6 in this study (Fig. 11D). These depressions are explained by normal fault reactivation during the ice advance and reverse faulting in postglacial times accompanied by the fall and rise of the salt wall, respectively (Huster *et al*. 2020). Contrary to the Bay of Kiel, Zechstein salt is absent in the area of the LFS. Thus, the development of such shallow depressions filled with postglacial sediments in this study did not involve salt movement and is only related to Quaternary fault reactivation.

Conclusions

This study presents key seismic reflection profiles from a densely spaced network of high-resolution seismic data offshore the northeastern coast of Langeland Island, which image a repeatedly reactivated WNW–ESE-striking fault system adjacent to an elevated basement block of the Ringkøbing–Fyn High. In combination with images showing the diffraction energy blended over time-migrated seismic reflection images, a precise fault analysis covering the Triassic to Quaternary subsurface reveals the character and spatial pattern of a series of Mesozoic–Cenozoic faults, which we refer to as the LFS. Sediment echosounder images of the uppermost part of the Quaternary succession enable the identification of

recent fault movements. Thus, the LFS represents a prime example of reoccurring tectonic activity with repeated fault reactivation along the margin of a complex intracontinental sedimentary basin. The main findings are as follows:

- The LFS consists of two approximately WNW–ESE-striking grabens bound by conjugate faults, whereas the southern graben joins the northern one in the central part of our study area. At a shallow level, the southern graben forms the offshore continuation of a Quaternary fault and graben structure observed onshore Langeland Island.
- The LFS is parallel to a branch of an elevated basement belonging to the Ringkøbing Fyn High, which developed owing to differential subsidence during the Triassic between the basement high and the faster subsiding adjacent North German and Norwegian–Danish basins. The southern flank of the high is bound by a fault that is rooted within the basement and was inverted during the Late Cretaceous.
- The Langeland Graben as identified in AEM-data correlates with the southern LFS.
- Initial Mesozoic faulting within the LFS occurred during the Triassic. Faults of the LFS were not inverted in Late Cretaceous time; rather, they show indications of repeated normal faulting during deposition of the Maastrichtian and Danian. Inversion was localized at the southern flank of the basement high. A possible explanation for this different structural style would be that the southward located basement high shielded the LFS from compression originating from the south.
- Faults of the LFS were reactivated during the Quaternary, as evident by the propagation of faults across the Quaternary sediments up to the sea floor. Lithological information from nearby wells suggests that the faulted Quaternary succession consists mostly of glacial and postglacial deposits. Accordingly, faulted strata visible within the uppermost succession of the Quaternary imaged by the sediment echosounder data indicate that faulting must have been in glacial or postglacial times. Thus, the LFS was reactivated over a length scale of a minimum 8.5 km. We discuss the Quaternary fault reactivation of the LFS in the context of glacially induced faulting owing to stress from glacially isostatic adjustments and the present-day stress field. Glacially induced fault reactivation seems plausible; however, a reactivation unrelated to glacially induced stress cannot be excluded. Future studies using, e.g., LiDAR data or modelling of glacially induced stress are needed to verify the origin of Quaternary fault reactivation within the LFS.
- Correlation of inherited deep-rooted faults with shallow faults in the Quaternary cover requires vertically continuous mapping of faults down to the sea floor (offshore) or ground surface (onshore). Since the geological structures of the Baltic Sea continue into the hinterland of the littoral states and comparable studies with similar seismic resolution are lacking there owing to the disproportionately higher operational effort, it can be assumed that the tectonic activity of deep-reaching faults in northern Europe during the Quaternary is more extensive than known. The approach used here of combining different geophysical data sets and methods from onshore and offshore provides a more detailed picture of the structures and their tectonic history. This helps to deepen our understanding of neotectonics and its connection with deep-seated tectonic structures.

Acknowledgements. – The authors would like to thank the editor Jan A. Piotrowski and the reviewers Christian Brandes and Peter B.E. Sandersen for their constructive comments that improved the manuscript. Captain Marc Petrokowski and his RV 'Alkor' crew were great in supporting our survey. The same applies to our technician Sven Winter. The authors would like to thank Benjamin Schwarz for providing the code for the diffraction separation. Further we thank Holger Lykke-Andersen and Egon Nørmark for providing the BaltSeis data (Fig. 5) which motivated our study. In addition, the authors are grateful to Schlumberger for providing VISTA seismic processing software and IHS Markit for providing KINGDOM seismic interpretation software under the umbrella of the University Grant Program. The work was funded by the Gefördert durch die Deutsche Forschungsgemeinschaft – 465329435. Open Access funding enabled and organized by Projekt DEAL.

Author contributions. – Conceptualization of this study was done by NA and CH. NA is the corresponding author and carried out seismic interpretation and mapping in this study. NA created the figures and was the primary writer of the manuscript. Structural interpretation and the discussion were primarily done by NA and CH. THRA reviewed and edited the manuscript. JP wrote the methodology subsection on the diffraction imaging, created Fig. 3 and helped with the interpretation of the diffraction images. LB carried out the seismic processing of the AL545 profiles. WS applied the diffraction separation algorithm. All authors contributed to the editing and reviewing of the manuscript.

Data availability statement. – Shown seismic data of the AL545 cruise (segy) and grids (ascii) are available via the Pangaea open access library (Ahlrichs *et al.* 2023).

References

Ahlers, S., Henk, A., Hergert, T., Reiter, K., Müller, B., Röckel, L., Heidbach, O., Morawietz, S., Scheck-Wenderoth, M. & Anikiev, D. 2021: 3D crustal stress state of Germany according to a data-calibrated geomechanical model. *Solid Earth 12*, 1777–1799.

Ahlrichs, N., Hübscher, C., Andersen, T. R., Preine, J., Bogner, L. & Schäfer, W. 2023: Time-migrated multichannel seismic data and separated diffraction energy, sediment echosounder data and calculated grids from the Langeland Fault System, Baltic Sea. *PANGAEA*. https://doi.org/10.1594/PANGAEA.954017.

Ahlrichs, N., Hübscher, C., Noack, V., Schnabel, M., Damm, V. & Krawczyk, C. M. 2020: Structural evolution at the northeast north German Basin margin: from initial Triassic salt movement to Late Cretaceous-Cenozoic remobilization. *Tectonics 39*, 1–26.

Ahlrichs, N., Noack, V., Hübscher, C., Seidel, E., Warwel, A. & Kley, J. 2021: Impact of Late Cretaceous inversion and Cenozoic extension on salt structure growth in the Baltic sector of the north German Basin. *Basin Research 34*, 220–250.

Ahlrichs, N., Noack, V., Seidel, E. & Hübscher, C. 2022: Triassic-Jurassic salt movement in the Baltic sector of the north German Basin and its relation to post-Permian regional tectonics. *Eartharxiv* [Preprint], https://doi.org/10.31223/X5WD3R.

Al Hseinat, M. & Hübscher, C. 2017: Late Cretaceous to recent tectonic evolution of the north German Basin and the transition zone to the Baltic Shield/Southwest Baltic Sea. *Tectonophysics 708*, 28–55.

Al Hseinat, M., Hübscher, C., Lang, J., Lüdmann, T., Ott, I. & Polom, U. 2016: Triassic to recent tectonic evolution of a crestal collapse graben above a salt-cored anticline in the Glückstadt Graben/north German Basin. *Tectonophysics 680*, 50–66.

Andersen, T. R., Westergaard, J. H. & Pytlich, A. 2016: Delineation of fault systems on Langeland, Denmark based on AEM data and boreholes. *ASEG-PESA AIG 1*, 1–6. ASEG-PESA-AIG, Adelaide.

Bendixen, C., Jensen, J., Bennike, O. & Boldreel, L. O. 2013: Late glacial to early Holocene development of southern Kattegat. *Geological Survey of Denmark and Greenland Bulletin 28*, 21–24.

Bennike, O., Jensen, J. B., Lemke, W., Kuijpers, A. & Lomholt, S. 2004: Late- and postglacial history of the Great Belt, Denmark. *Boreas 33*, 18–33.

Bertelsen, F. 1980: Lithostratigraphy and depositional history of the Danish Triassic. *Danmarks Geologiske Undersøgelser B 4*, 1–60.

Berthelsen, A. 1992: Tectonic evolution of Europe. From Precambrian to Variscan Europe. *In* Blum, M. D. (ed.): *A Continent Revealed: The European Geotraverse*, 153–164. Cambridge University Press, Cambridge.

Bhattacharya, P. K. & Patra, H. P. 1968: *Direct Current Geoelectric Sounding – Principles and Interpretation*. 135 pp. Elsevier, Amsterdam.

Björk, S. 1995: A review of the history of the Baltic Sea, 13.0-8.0ka BP. *Quaternary International 27*, 19–40.

Brandes, C., Plenefisch, T., Tanner, D. C., Gestermann, N. & Steffen, H. 2019: Evaluation of deep crustal earthquakes in northern Germany – possible tectonic causes. *Terra Nova 31*, 83–93.

Brandes, C., Polom, U., Winsemann, J. & Sandersen, P. B. E. 2022: The near-surface structure in the area of the Børglum fault, Sorgenfrei-Tornquist zone, northern Denmark: implications for fault kinematics, timing of fault activity and fault control on tunnel valley formation. *Quaternary Science Reviews 289*, 1–26.

Brandes, C., Steffen, H., Sandersen, P. B. E., Wu, P. & Winsemann, J. 2018: Glacially induced faulting along the NW segment of the Sorgenfrei–Tornquist Zone, northern Denmark: implications for neotectonics and Lateglacial fault-bound basin formation. *Quaternary Science Reviews 189*, 149–168.

Cartwright, J. 1990: The structural evolution of the Ringkøbing-Fyn High. *In* Blundell, D. J. & Gibbs, A. D. (eds.): *Tectonic Evolution of North Sea Rifts*, 200–2106. Oxford University Press, New York.

Clausen, O. & Pedersen, P. 1999: Late Triassic structural evolution of the southern margin of the Ringkøbing-Fyn High, Denmark. *Marine and Petroleum Geology 16*, 653–665.

Dadlez, R. & Marek, S. 1998: Major faults, salt- and non-salt anticlines. *In* Dadlez, R., Marek, S. & Pokorski, J. (eds.): *Paleogeographic Atlas of Epicontinental Permian and Mesozoic in Poland (1:2500000)*. Polish Geological Institute, Warszawa.

Ehlers, J., Eissmann, L., Lippstreu, L., Stephan, H.-J. & Wansa, S. 2004: Pleistocene glaciations of North Germany. *Developments in Quaternary Sciences 2*, 135–146.

Eiriksson, J., Kristensen, P. H., Lykke-Andersen, H., Brooks, K., Murray, A., Knudsen, K. L. & Glaister, C. 2006: A sedimentary record from a deep Quaternary valley in the southern Lillebælt area, Denmark: Eemian and early Weichselian lithology and chronology at Mommark. *Boreas 35*, 320–331.

Endler, M., Endler, R., Wunderlich, J., Bobertz, B., Leipe, T., Moros, M., Jensen, J. B. & Arz, H. W. 2016: Geo-acoustic modelling of late and postglacial sedimentary units in the Baltic Sea and their acoustic visibility. *Marine Geology 376*, 86–101.

Erlström, M. & Sivhed, U. 2001: Intracratonic dextral transtension and inversion of the southern Kattegat on the southwest margin of Baltica – Seismostratigraphy and structural development. *SGU Research Papers 832*, 1–31.

Erlström, M., Thomas, S., Deeks, N. & Sivhed, U. 1997: Structure and tectonic evolution of the Tornquist zone and adjacent sedimentary basins in Scania and the southern Baltic Sea area. *Tectonophysics 271*, 191–215.

EUGENO-S Working Group 1988: Crustal structure and tectonic evolution of the transition between the Baltic Shield and the north German Caledonides (the EUGENO-S Project). *Tectonophysics 150*, 253–348.

von Eynatten, H., Kley, J., Dunkl, I., Hoffmann, V.-E. & Simon, A. 2021: Late Cretaceous to Paleogene exhumation in central Europe – localized inversion vs. large-scale domal uplift. *Solid Earth 12*, 935–958.

Frahm, L., Hübscher, C., Warwel, A., Preine, J. & Huster, H. 2020: Misinterpretation of velocity pull-ups caused by high-velocity infill of tunnel valleys in the southern Baltic Sea. *Near Surface Geophysics 18*, 643–657.

Ford, J., Urgeles, R., Camerlenghi, A. & Gràcia, E. 2021: Seismic diffraction imaging to characterize mass-transport complexes: examples from the Gulf of Cadiz, south west Iberian Margin. *Journal of Geophysical Research: Solid Earth 126*, e2020JB021474, https://doi.org/10.1029/2020JB021474.

GEUS 2014: The GEUS Jupiter National Well database. Available at: https://eng.geus.dk/products-services-facilities/data-and-maps/national-well-database-jupiter (accessed 20.06.2022).

GEUS seismologi 2022: Registrerede jordskælv i Danmark. https://www.geus.dk/natur-og-klima/jordskaelv-og-seismologi/registrerede-jordskaelv-i-danmark (accessed 18.10.2022).

Graversen, O. 2006: The Jurassic-Cretaceous North Sea rift dome and associated basin evolution. *AAPG Search and Discovery 30040*, 19–22.

Guterch, A., Wybraniec, S., Grad, M., Chadwick, A., Krawczyk, C., Ziegler, P. A., Thybo, H. & De Vos, W. 2010: Crustal structure and structural framework. *In* Doornenbal, H. & Stevenson, A. (eds.): *Petroleum Geological Atlas of the Southern Permian Basin Area*, 11–23. EAGE Publications, Houten.

Hansen, M. & Pjetursson, B. 2011: Free, online Danish shallow geological data. *Geological Survey of Denmark and Greenland Bulletin 23*, 53–56.

Hansen, T. H., Clausen, O. R. & Andresen, K. J. 2021: Thick- and thin-skinned basin inversion in the Danish central Graben, North Sea – the role of deep evaporites and basement kinematics. *Solid Earth 12*, 1719–1747.

Hansen, M. B., Lykke-Andersen, H., Dehghani, A., Gajewski, D., Hübscher, C., Olesen, M. & Reicherter, K. 2005: The Mesozoic–Cenozoic structural framework of the Bay of Kiel area, western Baltic Sea. *International Journal of Earth Sciences 94*, 1070–1082.

Hansen, M. B., Scheck-Wenderoth, M., Hübscher, C., Lykke-Andersen, H., Dehghani, A., Hell, B. & Gajewski, D. 2007: Basin evolution of the northern part of the northeast German Basin—insights from a 3D structural model. *Tectonophysics 437*, 1–16.

Heidbach, O., Rajabi, M., Cui, X., Fuchs, K., Müller, B., Reinecker, J., Reiter, K., Tingay, M., Wenzel, F., Xie, F., Ziegler, M. O., Zoback, M.-L. & Zoback, M. 2018: The world stress map database release 2016: crustal stress pattern across scales. *Tectonophysics 744*, 484–498.

Hoth, K., Rusbült, J., Zagora, K., Beer, H. & Hartmann, O. 1993: Die tiefen Bohrungen im Zentralabschnitt der Mitteleuropäischen Senke – Dokumentation für den Zeitabschnitt 1962-1990. *Verlag der Gesellschaft für Geologische Wissenschaften 2*, 1–145.

Houmark-Nielsen, M. 1987: Pleistocene stratigraphy and glacial history of the central part of Denmark. *Bulletin of the Geological Society of Denmark 36*, 1–189.

Huang, L. & Liu, C. Y. 2017: Three types of flower structures in a divergent-wrench fault zone. *Journal of Geophysical Research: Solid Earth 122*, 10478–10497.

Hübscher, C., Aster, M. S., Behr, C., Bogner, L., Chung, J. I., Decdariani, A., Dittmers, C., Ehlies, V., Eßbach, V., Häcker, T., Lackner, M., Maaß, R., Preine, J., Rehm, A., Uhl, K. J. & Wodke, V. 2020: Studierendenbericht zum Seepraktikum Geophysik 2020 (UHH). *ALKOR-Berichte*, 1–5. Institut für Geophysik, Hamburg. Available at: https://oceanrep.geomar.de/id/eprint/50628/.

Hübscher, C., Hansen, M. B., Triñanes, S. P., Lykke-Andersen, H. & Gajewski, D. 2010: Structure and evolution of the northeastern German Basin and its transition onto the Baltic Shield. *Marine and Petroleum Geology 27*, 923–938.

Hübscher, C., Lykke-Andersen, H., Hansen, M. & Reicherter, K. 2004: Investigating the structural evolution of the western Baltic. *Eos 85*, 115.

Hughes, A. L. C., Gyllencreutz, R., Lohne, Ø. S., Mangerud, J. & Svendsen, J. I. 2016: The last Eurasian ice sheets – a chronological database and time-slice reconstruction, DATED-1. *Boreas 45*, 1–45.

Huster, H., Hübscher, C. & Seidel, E. 2020: Impact of Late Cretaceous to Neogene plate tectonics and Quaternary ice loads on supra-salt deposits at eastern Glückstadt Graben, north German Basin. *International Journal of Earth Sciences 109*, 1029–1050.

Japsen, P., Bidstrup, T. & Lidmar-Bergström, K. 2002: Neogene uplift and erosion of southern Scandinavia induced by the rise of the south Swedish Dome. *In* Doré, A. G., Cartwright, J. A., Stoker, M. S., Turner, J. P. & White, N. (eds.): *Exhumation of the North Atlantic Margin: Timing, Mechanisms and Implications for Petroleum Exploration*, 183–207. Geological Society, London.

Japsen, P., Green, P. F., Nielsen, L. H., Rasmussen, E. S. & Bidstrup, T. 2007: Mesozoic-Cenozoic exhumation events in the eastern North Sea Basin: a multi-disciplinary study based on palaeothermal, palaeoburial, stratigraphic and seismic data. *Basin Research 19*, 451–490.

Jørgensen, F. & Sandersen, P. B. E. 2006: Buried and open tunnel valleys in Denmark—erosion beneath multiple ice sheets. *Quaternary Science Reviews 25*, 1339–1363.

Kammann, J., Hübscher, C., Boldreel, L. O. & Nielsen, L. 2016: High-resolution shear-wave seismics across the Carlsberg fault zone south of Copenhagen – implications for linking Mesozoic and late Pleistocene structures. *Tectonophysics 682*, 56–64.

Kley, J. 2018: Timing and spatial patterns of Cretaceous and Cenozoic inversion in the southern Permian Basin. *Geological Society, London, Special Publications 469*, 19–31.

Kley, J. & Voigt, T. 2008: Late Cretaceous intraplate thrusting in central Europe: effect of Africa-Iberia-Europe convergence, not Alpine collision. *Geology 36*, 839–842.

Kley, J., Franzke, H.-J., Jähne, F., Krawczyk, C., Lohr, T., Reicherter, K., Scheck-Wenderoth, M., Sippel, J., Tanner, D., van Gent, H. & Group, t. S. S. G 2008: Strain and stress. *In* Littke, R., Bayer, U., Gajewski, D. & Nelskamp, S. (eds.): *Dynamics of Complex Intracontinental Basin System, the central European Basin System*, 97–124. Springer Verlag, Berlin, Heidelberg.

Kockel, F. 2003: Inversion structures in central Europe – expressions and reasons, an open discussion. *Netherlands Journal of Geosciences – Geologie en Mijnbouw 82*, 367–382.

Krzywiec, P. 2006: Structural inversion of the Pomeranian and Kuiavian segments of the mid-polish trough – lateral variations in timing and structural style. *Geological Quarterly 50*, 151–168.

Landa, E. & Keydar, S. 1998: Seismic monitoring of diffraction images for detection of local heterogeneities. *Geophysics 63*, 1093–1100.

Lykke-Andersen, H. 1992: Massebevægelser i Vendsyssels og Kattegats kvartære aflejringer [mass movements in the Quaternary deposits of Vendsyssel and the Kattegat]. *Dansk Geologisk Forening Årsskrift for 1990–91*, 93–97.

Lykke-Andersen, H., Madirazza, I. & Sandersen, P. B. E. 1996: 1996: Tektonik og landskabsdannelse i Midtjylland [Tectonics and landscape formation in mid-Jutland]. *Geologisk Tidsskrift 3*, 1–32.

Maystrenko, Y., Bayer, U., Brink, H.-J. & Littke, R. 2008: The central European Basin system – an overview. *In* Littke, R., Bayer, U., Gajewski, D. & Nelskamp, S. (eds.): *Dynamics of Complex Intracontinental Basins, the Central European Basin System*, 17–34. Springer Verlag, Berlin, Heidelberg.

Michelsen, O. 1978: Stratigraphy and distribution of Jurassic deposits of the Norwegian-Danish basin. *Danmarks Geologiske Undersøgelse Serie B*, 1–28.

Müller, K., Winsemann, J., Tanner, D. C., Lege, T., Spies, T. & Brandes, C. 2021: Glacially induced faults in Germany. *In* Steffen, H., Olesen, O. & Sutinen, R. (eds.): *Glacially Triggered Faulting*, 283–303. Cambridge University Press, Cambridge.

Nielsen, L. H. & Japsen, P. 1991: Deep wells in Denmark – 1935-1990. *Danmarks Geologiske Undersøgelse Serie A*, 1–179.

Peacock, D. C. P. & Banks, G. J. 2020: Basement highs: definitions, characterisation and origins. *Basin Research 32*, 1685–1710.

Pharaoh, T., Dusar, M., Geluk, M., Kockel, F., Krawczyk, C., Krzywiec, P., Scheck-Wenderoth, M., Thybo, H., Vejbæk, O. V. & van Wees, J.-D. 2010: Tectonic evolution. *In* Doornenbal, H. & Stevenson, A. G. (eds.): *Petroleum Geological Atlas of the Southern Permian Basin Area*, 25–57. EAGE Publications, Houten.

Preine, J., Schwarz, B., Bauer, A. & Hübscher, C. 2020: When there is No offset: a demonstration of seismic diffraction imaging and depth-velocity model building in the southern Aegean Sea. *Journal of Geophysical Research: Solid Earth 125*, e2020JB019961, https://doi.org/10.1029/2020JB019961.

Rasmussen, E. S. 2009: Neogene inversion of the central Graben and Ringkøbing-Fyn High, Denmark. *Tectonophysics 465*, 84–97.

Reinhold, K., Krull, P., Kockel, F. & Rätz, J. 2008: *Salzstrukturen Norddeutschlands: Geologische Karte. 1:500000*. Bundesanstalt für Geowissenschaften und Rohstoffe, Hannover.

Sachse, V. F. & Littke, R. 2016: Burial, temperature and maturation history of the Ringkøbing-Fyn High, Denmark. *Zeitschrift der Deutschen gesellschaft für Geowissenschaften (ZDDG) – Journal of Applied and Regional Geology 167*, 249–268.

Sandersen, P. B. E. & Jørgensen, F. 2015: Neotectonic deformation of a late Weichselian outwash plain by deglaciation-induced fault reactivation of a deepseated graben structure. *Boreas 44*, 413–431.

Sandersen, P. B. E., Gregersen, S. & Voss, P. H. 2021: Lateglacial and postglacial faulting in Denmark. *In* Steffen, H., Olesen, O. & Sutinen, R. (eds.): *Glacially Triggered Faulting*, 263–282. Cambridge University Press, Cambridge.

Schwarz, B. 2019a: Chapter one – an introduction to seismic diffraction. *In* Schmelzbach, C. (ed.): *Advances in Geophysics*, 1–64. Elsevier, Cambridge.

Schwarz, B. 2019b: Coherent wavefield subtraction for diffraction separation. *Geophysics 84*, V157–V168.

Schwarz, B. & Gajewski, D. 2017: Accessing the diffracted wavefield by coherent subtraction. *Geophysical Journal International 211*, 45–49.

Schwarz, B. & Krawczyk, C. M. 2020: Coherent diffraction imaging for enhanced fault and fracture network characterization. *Solid Earth 11*, 1891–1907.

Sirocko, F., Reicherter, K., Lehné, R., Hübscher, C., Winsemann, J. & Stackebrandt, W. 2008: Glaciation, salt and the present landscape. *In* Littke, R., Bayer, U., Gajewski, D. & Nelskamp, S. (eds.): *Dynamics of Complex Intracontinental Basins, the Central European Basin System*, 233–245. Springer Verlag, Berlin, Heidelberg.

Steffen, R. & Steffen, H. 2021: Reactivation of non-optimally orientated faults due to glacially induced stresses. *Tectonics 40*, e2021TC006853, https://doi.org/10.1029/2021TC006853.

Steffen, H., Olesen, O. & Sutinen, R. 2021a: Glacially triggered faulting – a historical overview and recent developments. *In* Steffen, H., Olesen, O. & Sutinen, R. (eds.): *Glacially Triggered Faulting*, 3–19. Cambridge University Press, Cambridge.

Steffen, R., Wu, P. & Lund, B. 2021b: Geomechanics of glacially triggered faulting. *In* Steffen, H., Olesen, O. & Sutinen, R. (eds.): *Glacially Triggered Faulting*, 20–39. Cambridge University Press, Cambridge.

Stemmerik, L., Frykman, P., Winther Christensen, O. & Stentoft, N. 1987: The Zechstein carbonates of southern Jylland, Denmark. *In* Brooks, J. & Glennie, K. (eds.): *Petroleum Geology of North West Europe*, 365–374. Graham & Trotman, London.

Thomsen, E. 1974: Maastrichtian and Danian facies pattern on the Ringkøbing-Fyn High, Denmark. *Bulletin of the Geological Society of Denmark 23*, 118–123.

Thomsen, R., Søndergaard, V. H. & Sørensen, K. I. 2004: Hydrogeological mapping as a basis for establishing site-specific groundwater protection zones in Denmark. *Hydrogeology Journal 12*, 550–562.

Thybo, H. 1997: Geophysical characteristics of the Tornquist fan area, northwest trans-European suture zone: indication of late carboniferous to early Permian dextral transtension. *Geological Magazine 134*, 597–606, https://doi.org/10.1017/S0016756897007267.

Thybo, H. 2001: Crustal structure along the EGT profile across the Tornquist fan interpreted from seismic, gravity and magnetic data. *Tectonophysics 334*, 155–190.

Underhill, J. R. 1998: Jurassic. *In* Glennie, K. W. (ed.): *Petroleum Geology of the North Sea: Basic Concepts and Recent Advances*, 245–293. Blackwell Science, Malden.

Vejbæk, O. V. 1997: Dybe strukturer i danske sedimentære bassiner. *Geologisk Tidsskrift 4*, 1–31.

Vejbæk, O. V. & Andersen, C. 2002: Post mid-Cretaceous inversion tectonics in the Danish central Graben – regionally synchronous tectonic events? *Bulletin of the Geological Society of Denmark 49*, 129–144.

Vejbæk, O. V., Andersen, C., Dusar, M., Herngreen, W., Krabbe, H., Leszczynski, K., Lott, G. K., Mutterlose, J. & van der Molen, A. S. 2010: Cretaceous. *In* Doornenbal, J. C. & Stevenson, A. G. (eds.): *Petroleum Geological Atlas of the Southern Permian Basin Area*, 195–209. EAGE Publications, Houten.

Vinken, R. & International Geological Correlation Programme 1988: *The Northwest European Tertiary Basin: Results of the International Geological Correlation Programme Project no. 124*. 508 pp. Bundesanstalt für Geowissenschaften und Rohstoffe, Hannover.

Warsitzka, M., Jähne-Klingberg, F., Kley, J. & Kukowski, N. 2019: The timing of salt structure growth in the southern Permian Basin (central Europe) and implications for basin dynamics. *Basin Research 31*, 337–360.

White, S. H., Bretan, P. G. & Rutter, E. H. 1986: Fault-zone reacctivation: kinematics and mechanisms. *Philosophical Transactions of the Royal Society of London A317*, 81–97.

Winn, K. 1974: Present and postglacial sedimentation in the Great Belt channel (Western Baltic). *Meyniana 26*, 63–101.

Wu, P. & Peltier, W. R. 1982: Viscous gravitational relaxation. *Geophysical Journal of the Royal Astronomical Society 70*, 435–486.

Wunderlich, J. & Müller, S. 2003: High-resolution sub-bottom profiling using parametric acoustics. *International Ocean Systems 7*, 6–11.

Ziegler, P. A. 1990: *Geological Atlas of Western and Central Europe*. 239 pp. Shell Internationale Petroleum Maatschappij B. V, The Hague.